To the Graduate Council:

I am submitting herewith a thesis written by Satyavani Bari entitled “Moiré Fringe analysis of accuracy of nano metrology in the SEM.” I have examined the final electronic copy of this thesis for form and content and recommend that it be accepted in partial fulfillment of the requirement for the degree of Master of Science with a major in Material Science and Engineering.

David C Joy, Major Professor

We have read this thesis and
recommend its acceptance:

Philip D Rack
_____

Gerd Duscher
_____

Accepted for the Council:

Carolyn R. Hodges
Vice Provost and Dean of the Graduate School

(Original signatures are on file with official student records.)

Moiré Fringe analysis of accuracy of nano metrology in the SEM.

A Thesis
Presented for the
Master of Science
Degree
The University of Tennessee, Knoxville

Satyavani Bari
May 2009

Abstract

Image based metrology for Scanning electron microscope (SEM) has become most important, versatile, and widely employed techniques for metrology as the 'Critical Dimension' scale has been reduced from micrometer to nanometers. However, the image that is captured and displayed by the SEM is not guaranteed to be true representation of the actual structure especially at nano meter level because, the factors that may be of little importance at micrometer level may induce substantial at nanometer level. One major problem in the measurement made using SEM is that the field of view of the image is calculated - based on the data provided by the manufacturer on beam energy, working distance current flowing through the scan coils – rather than measured. As a result the two measurements of an object made by identical instruments under same instrument are likely to result in significantly different values of the sizes of same feature. Accurate metrology in the size range from nanometer to micrometer requires access to traceable artifacts of know size length. In this thesis a procedure for the calibration of the imaging field of view using a specially fabricated traceable standard artifact by moiré fringe technique is developed and demonstrated.

The SEM is a mapping - rather than imaging - instrument so the accuracy of the geometric mapping of the image data from specimen to the display screen is crucial to the accuracy of the SEM image based metrology. Non-linearities in the raster depend on the scan speed an on the magnitude on the scan current so, consequently, the apparent size of the objects in the display may vary depending on the where in the field of the view they appear. In addition the X and Y axes of the raster scan may not be orthogonal, and the magnification of an object

may vary with time if the specimen itself is charging. This thesis develops a novel technique using moiré fringes which permit such errors to detect and quantified.

TABLE OF CONTENTS

LIST OF FIGURES

CHAPTER 1

INTRODUCTION

1.1 Introduction

The performance, and the monetary value, of semiconductor devices depends directly on their exact physical size ('Critical dimensions') so every day millions of critical dimensions are measured by analyzing images of area of interest recorded by scanning electron microscopes(SEM). The aim of this thesis is to demonstrate that the accuracy and precision of such measurements is inherently degraded because of the absence of appropriate calibration procedures and by the presence of significant errors in the process which maps the sample are to the display screen of the SEM. It is proposed that moiré fringes provide a sensitive and quantitative way to detect and correct such problem.

From the revolutionary invention of the transistor in 1947 until today, the semiconductor industry continuously reduced the size of integrated circuits from the micrometer level, first to the sub-micrometer level, and now to the nanometer scale. This miniaturization in the device design rules has both increased the performance of the circuits and decreased their cost drastically. The dimension of the each component on the chip of electronic device directly influences the performance and the cost of the device. It is known that a 10nm difference in size causes a measurable change in speed of the microprocessor, which in turn can lead to a drop in the selling price of $100 or more for the device [1]. Considering the millions of microprocessors that are sold annually, the economic value per nanometer is of the order of billions of dollars.

However while performance improves with the decreasing size, the demands on the accuracy and reliability of the component dimensions become extremely severe.

This reduction in the size of the components has required the development of various advanced and sophisticated manufacturing processes like Extreme Ultra Violet (EUV) Lithography, Nanoimprint Lithography, and Immersion Lithography, although the common mass production process is still Photolithography. In order to control the fabrication process the size, shape, and spacing of critical portions of the device such as the gate region must be measured to ensure that they fall within the required range. 'Critical dimensional metrology' the measurement and monitoring of these critical dimensions is therefore equally crucial at nanometer level. Optical metrology has long been employed to perform critical dimensional metrology for larger than 1μm, but as CD decreased from micrometer to sub-micrometer level, critical dimension metrology migrated to advanced instruments like the scanning electron microscope (SEM), atomic force and scanning probe microscopes [2]. The imaging magnification of the SEM or any other instrument, like that used for metrology must frequently be checked and calibrated, to address this issue, National Institute of Standards and Technology (NIST) have made calibration artifacts that have the status of traceable standards and are known as Standard Reference Materials (SRM). The various standards made by NIST could not be updated at the same rate as the development of the manufacturing technologies [3] so the semiconductor industry is investing millions of dollars in research for developing calibration standards, appropriate scientific instrumentation, and for evaluation of the present measurement procedures [5].

Because the most common instrument used for device metrology at this time is the 'Critical Dimension SEM (CD-SEM)' this thesis will concentrate on this device. However much of the work described is equally applicable to other tools such as Atomic Force Microscopes.

1.2 Scanning Electron Microscope

The Scanning Electron microscope produces an image by scanning the sample surface in raster scan pattern with high energy beam of electrons. Around 50,000 SEMs are in daily operation worldwide for research in many areas of science and in the nanotechnology and semiconductor industries. The features that make SEM the most widely used high performance microscope are its large depth of focus, which enables large area of sample to be focused, its higher ultimate magnification and its resolution. These benefits are possible because the resolution of any microscope is, according to Abbe theorem, a function of the wavelength (λ) of the illuminating beam and the wavelength of the electron is of order 0.002 nm to 0.1 nm for energies in the 1 to 30keV range in addition electrons have the strongest interaction with matter of any radiation and so provide many types of information about the sample.

The first instrument recognizable as a Scanning Electron Microscope was built in 1935 in German by Max Knoll. Ever since then, the tool has been continuously improved to keep up with the ever rising demand for imaging, micro analytical and measuring capabilities with higher resolution.

1.2.1 Overview of working of SEM

The working principle of the SEM, and of related instruments such as the scanning probe microscope or the atomic force microscope, is illustrated in Figure 1. In SEM, The sample is examined by scanning an area, pixel by pixel, and reconstructing the same data on to the display screen one pixel at a time. The electron beam is generated from electron gun maintained in a vacuum environment. The beam is directed down to the sample surface following a vertical path through electromagnetic lenses. The incident beam interacts with the sample generating secondary electrons (SE), back scattered electrons (BSE), X-rays, Auger electrons, as well as

assorted optical, thermal and acoustic signals. These various emissions are collected by detectors, then amplified and processed to enhance contrast and brightness in the image produce the final image on a display screen of some type.

1.2.2 Important Components of a SEM

Electron Gun: The beam generation is the function of the electron gun. The emission of the electron beam depends on the type of the emitter employed and there are two types in common use - Thermionic emission and Field emission

Thermal emission generates the electron by exciting the filament through heating. Field emission is temperature independent and generates the electrons in an ultra high vacuum environment by extracting electrons from a sharp tip under the influence of a strong electrostatic field. Field emission is most commonly preferred for its small source size, high brightness and long life while thermionic sources offer simplicity, low cost, and large beam currents [6].

Lenses: Electrons are focused by electromagnetic lenses in which current passed in coils of copper wires creates magnetic fields., These electromagnetic lenses in the SEM are used both as Condenser lenses, to reduce the beam diameter, or as an Objective lens which focuses the beam on to the specimen Scan coils, generating magnetic fields in the X and Y directions deflect the electrons across the sample surface in a rectangular scan raster pattern [6].

Detector: The detectors are responsible for collecting the signal components from which the image is created. The most common detectors used are the Everhart-Thornley (E-T) detector and Backscattered (BSE) electron detector. The E-T contains a scintillator which converts the secondary electron signal into light which is the then amplified by a photo-multiplier. The backscattered detectors collect the electrons that ‘bounce’ back from the surface of the sample. The amplified signals are then sent to the display screen. The visual image on the

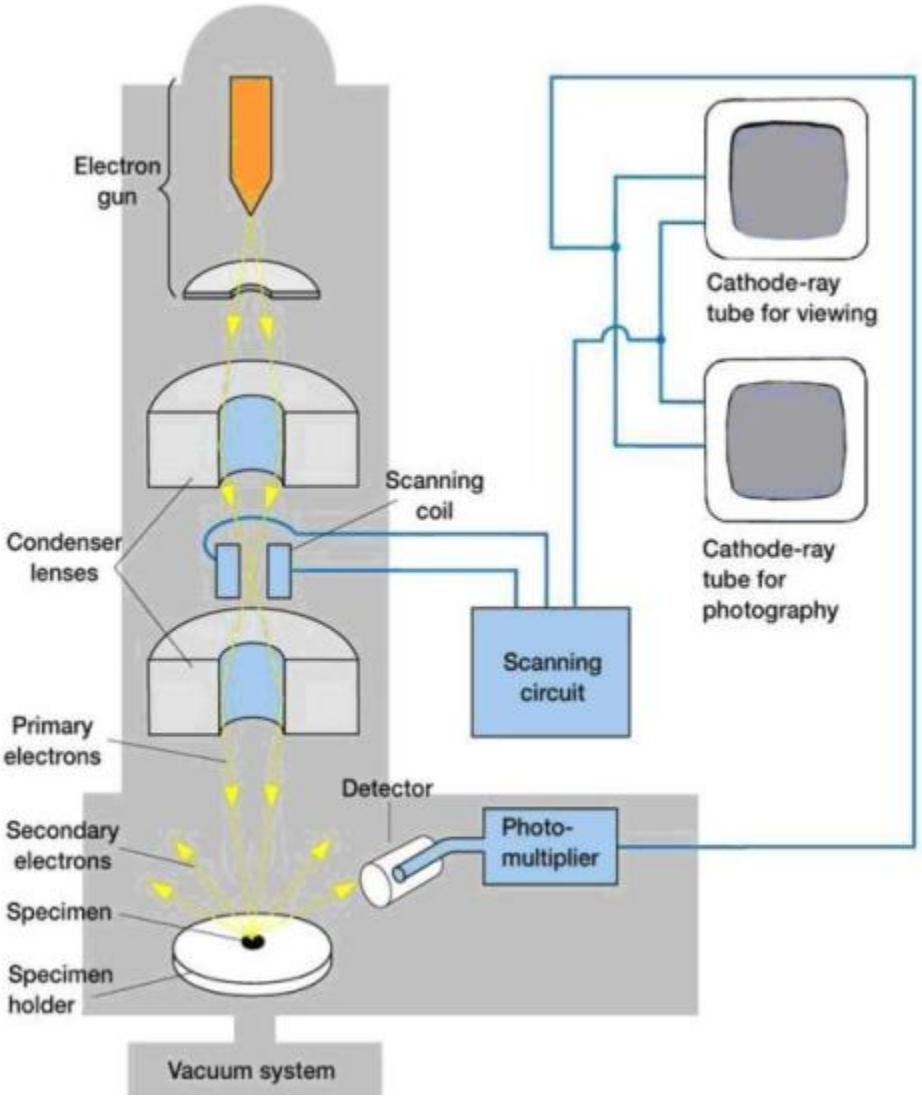

Figure 1: Schematic of SEM (taken from Dr. Joy SEM course Lecture Notes) [7].

viewing screen can display a wide variety of the information about the surface that has been scanned by the beam [6].

1.3 Metrology

The term Metrology is a Greek work meaning 'the study or science of measurements'. A core concept of metrology is the traceability, which implies that the measurement has been made by reference to or comparison with some object whose size is known relative to some physical standard – such as the wavelength of light – of internationally agreed magnitude. Calibration is an act of verifying the accuracy of the measurement by reference to a convenient artifact [8]. Metrology can be classified into three sub categories Scientific, Industrial, and Legal Metrology. Research and development involving the introduction of new measurement units, identification of the measurement standards and making them available for public use is defined as scientific metrology. Industrial metrology can be defined as application of the measurements to achieve the calibration of the instruments used to control manufacturing and industrial applications. Legal metrology is the concerned with writing, distributing and enforcing rules for the measurement standards and measuring instruments [8].

Metrology being thus described, its application in the semiconductor industry can be considered as the essential step to achieve control and reproducibility in a manufacturing process. Metrology has always been a very important area in the semiconductor industry as the size of each feature on the device would significantly affect the performance and the price of the device. As mentioned earlier by Ausschnitt and Lagus [1], it is the fact that even just a few nm change in the feature size of a device would lead to an unwanted change in the speed of the processor, which would make a difference of perhaps 100$ in the selling price of the device. The increasing application of industrial manufacturing technology of the device in nanometer range

has not been matched by an equal increase in the development of metrological instruments and calibration standards. The National Institute of Standards and Technology (NIST) has identified the crucial need for metrology in semiconductor manufacturing industry and initiated a National Semiconductor Metrology Program (NSMP) in 1992 [9]. NSMP has been grouped into various individual projects as Lithography Metrology, Critical Dimensional and Overlay Metrology, Interconnect and Packaging Metrology, Wafer Characterization and process Metrology, Test Metrology and Manufacturing Support. These individual projects all together lead to a single goal of achieving accuracy, precision, traceability and calibration standards [9].

The revolution in the semiconductor industry started with the decrease in the feature size from micrometer to sub-micron and currently to the nanometer range has made it challenging to achieve calibrated standard for metrology. Various metrology tools have been developed in order to reach the desired accuracy at the sub micrometer to nanometer range including Critical Dimension Scanning electron microscope (CD-SEM), Critical Dimension Atomic Force Microscope (CD-AFM), Scanning probe microscopes, Scanning near field optical microscope (SNOP), Spectroscopy, interferometry and Scatterometry, to name a few. Metrology performed at the mass production level is categorized into two types' in-line metrology and off-line metrology. Metrologies systems forming part of the manufacturing process are known as in-line metrology while metrology performed outside of the manufacturing process on different workspace are defined as off-line metrology. As of now only optical scatterometry is considered as being in-line metrology. The CD-SEM, CD-AFM are used for exclusively off-line metrology. Among all the tools available, the CD-SEM and CD-AFM are considered as those best capable of satisfying the present needs of the nanotechnology although the problems of damage due to the electron beam irradiation, and effects associated with beam induced charging often limit the

practical application of the technology. Since SEM is capable of high resolution imaging and high imaging speed it is considered to be a specialized tool for metrology [10]. The beam current, beam energy, and spot size are some of the parameters, which decide the image resolution. Also damage due to the electron beam irradiation, and effects associated with beam induced charging also play key roles in determining the quality of critical dimension measurement at the nanometer scale.

The most common method of CD measurement is 'image based metrology' i.e. determining size by a measurement from the image captured by the SEM but this should not be taken to imply that the size and shape obtained from a measurement of the SEM image is either accurate or reliable [10]. Minor errors in large size patterns may lead to major errors when considered at nanometer scale. A significant problem is that the indicated image magnification and field of view of the SEM is not derived from a calibration procedure but rather is calculated on the basis of preset parameters such as the beam energy , and the working distance of the sample. Hence two images of the same feature recorded on successive days from the same machine and under identical condition would most likely generate significantly different information about the size and shape of the object of interest. Therefore there is a need to develop traceable and portable length scale artifacts with sizes in the nanometer to micrometer range to permit calibration on demand for each image.

The SEM, AFM and STM, is a device which maps object data one pixel at a time on to a display screen. The inherent assumption is that this mapping operation is perfect, with the object and mapped image related by a single scaling constant. In fact the mapping process displays many problems including different magnification factors along the X and Y axes, non-linearities in either the X or Y direction, and a lack of orthogonality between the X and Y direction.

Consequently the image as displayed is not just modified by a magnification factor but is distorted by the non-linearity and poor orthogonality of the transfer process. It is the aim of the work described here to detect and quantify such mapping errors by using a novel method Moiré fringes-so that the accuracy of image based metrology can be improved.

1.3.1 Relation between moiré fringes and metrology

Moiré (French for 'mashed' or 'mixed') fringes are generated when two high periodic structures interfere with each other. This interference of patterns has long been of importance in optical metrology because extremely sensitivity to distortions and non-linearity can be achieved with minimal equipment. The basic moiré fringes are additive, subtractive, multiplicative and division moiré fringes, and will be discussed in detail in later chapters. Moiré fringes were used for decades to perform analysis of stress and strain in materials. Use of moiré fringes in metrology was first introduced during nineteenth century, when A.A. Michelson used this principle to build an 'interferometer' in 1870 [11].

In the conventional optical case moiré fringes are the result of interferences between two periodic physical structures. In the SEM, or AFM, moiré fringes are the result of interactions between a physical structure and the *virtual periodicity* of the scanned raster display. As a result any change in the raster - such as its size or direction – will affect the interference pattern generated. It is this sensitivity to geometry which makes it possible to observe and quantify distortions in the SEM image.

1.4 Scope of the project

In the present work, a commercial specimen (MetroBoost Inc: Santa Clara, CA) , consisting of poly-crystalline silicon wafer with a thin layer of oxide over it and containing

many high frequency line grating fabricated by mask lithography is used to detect and to suggest possible calibration standards to rectify mapping errors in the SEM. The high frequency gratings on the sample have been utilized to generate moiré fringes, when viewed under Scanning electron microscope. The main purpose of the project is to identify the possible mapping errors in scanning electron microscope using the moiré fringes created by the interference of the high frequency grating line and the raster scan of the SEM. Some of the mapping errors which could be identified are magnification errors, non linearity, and non orthogonality of the X and Y scan axis, and distortions in the image shape and size due to charging and contamination. The results obtained in this work can also be applicable to any other raster scan imaging as the principle behind imaging is same, for example instruments like Atomic force microscope (AFM).

CHAPTER 2

LITERATURE SURVEY

In this chapter, the rationale for nano-metrology, previous work and the current trends in the area of metrology in semiconductor industry are discussed. In addition a brief introduction on the origin and usage of moiré fringes is given. Finally the methodologies presented in the literature to identify and rectify the mapping errors in SEM are discussed.

2.1 Metrology in semiconductor industry

For the large scale production of transistors and integrated circuits whose size is always decreasing, it is necessary to ensure the performance of the device. This is achieved by measuring the 'critical dimensions' (CD) of a device and ensuring that the value falls within the boundaries set for optimum performance. Critical dimensions can include the size of the transistor gate, line width, line pitch, and pattern placement accuracy on the wafer. Hence, the metrology, the science and study of measurement plays a critical role in the semiconductor industry.

Metrology has been important every since the first the transistor was build, but it has gained even more importance as the size of the transistor gate has been reduced in the quest for higher switching speed. In turn, reducing the size of devices makes it possible to place more on a silicon wafer of given size which both reduces manufacturing costs while enhancing the potential abilities of the chips. This progression is often described as 'Moore's law' (from an essay by Gordon Moore one of the founders of Intel in 1965) although it is in fact just an observation that

the increasing the number of chips on a wafer by decreasing their size offers benefits both performance and the profits that can be generated.

To accommodate the exponentially increasing number of transistors on to single wafer, the size of the transistor is reduced drastically from 90nm in 2005 to 45nm currently with still further reduction underway to 22nm by 2016. In addition the wafer size is expected to increase from 300mm currently to 450mm in diameter for next transition [12]. As a consequence of the gate size approaching the sub-22nm scale predicted by International Technology Roadmap of Semiconductors (ITRS), the metrology capabilities of the present generation SEMs will be severely challenged.

Based on probable path of the semiconductor industry over next 15 years, ITRS has predicted that transistor gate CD might ultimately become less than 10nm before radical new technologies are available. Due to this rate of development in the manufacturing technology, there will be huge demand for the new measurement techniques [12]. Consequently to supplement the CD SEM and Scatterometry techniques now in use, the National Institute of Standards and Technology (NIST) is exploring new approaches such as Scatterfield microscopy and Small Angle X-ray Scattering (SAXS) [13].

Critical dimension metrology tools can be categorized in to two classes based on the technique they employ for measurement. The first group comprises instruments that perform metrology based on an image, the second those which derive dimensional information from the scattering and diffraction measurements. Thus SEM and AFM are image based metrology tools while tools such as Optical Scatterometers, Scatterfield microscopes, and small angle X-ray systems rely on the analysis of diffracted or scattered signal data [13]. Image based metrologies have the advantage that they can perform a measurement on a single, or even unique, artifact.

Scatter based systems, in contrast, must measure relatively large areas of a structure but offer high precision and speed. Table 1 [15] summarizes the strength and weaknesses of each of the available metrology tools.

It is necessary to have so many metrology tools and methods, because no one tool can provide all the required information. To quantify and compare the precision and repeatability of the metrology tools, factors such as relative accuracy, absolute accuracy, the influence of line edge roughness, sampling problems and consequential damage produced by measurement also needs to be considered. One method proposed to evaluate measurement tools and techniques, is to compare their measurement errors when they are applied to international metrology reference standard. This measurement of error is called as measurement uncertainty and can be obtained by comparison of measurement to measurement, tool to tool, sample to sample results using protocols defined by NIST and ITRS [14]. Continuous research in metrology has lead to development of many tools and techniques over the period of time. Major metrology methods for measurement uncertainty as classified by NIST and ITRS can be listed as:

1. Lithography metrology: Measurements of dimensions such as width, depth, shape and size of the patterns. Photo resist, phase shifters, anti reflective coating (ARC's) control the pattern dimension and shape, so characterization of these materials is also considered as part of lithography metrology [14].
2. Critical dimension and overlay metrology: Measurement of critical dimension of the pattern and positioning of the pattern on the wafer are function of CD and overlay metrology [14].

Table 1: Comparison of Metrology Tools [13]

Method	Strength	Weakness
Scanning Electron Microscopy	• High throughput • Measure both repeating and individual structures • Measures line edge roughness	• Requires Vacuum • Shrinkage • Requires simple modeling
Atomic Force Microscopy	• Measures both repeating and individual structures • Measures sidewall surface • Measure line edge roughness	• Low throughput • Tip-wear and crashes • Modeling for tip deconvolution required
Optical Scatterometry	• High throughput • Non-destructive • Measures average of many lines	• Requires complex modeling • Requires special metrology targets
Optical Scatterfield Microscopy	• High throughput • Non-destructive • Average of many lines • Simultaneous overlay • Small target size	• Immature technology • Requires complex modeling • Requires special metrology targets
Small angle X-ray Scattering	• Accurate • Overlay of hidden features • Line edge and width roughness • Measures average and variance over multiple lines • Simple analysis	• Need of high brightness sources which are only synchrotrons • Lab sources are 3 orders of magnitude less brightness • Requires metrology targets larger than those for optical Scatterometry

3. Interconnect metrology: Measurement of the interconnect structures that connect the IC structures to the silicon on the board. Measurement of sidewalls of trenches and vias are major components of the interconnect metrology [14].
4. Front End Processes metrology: Measurement of parameters in wafer possessing techniques such as wafer flatness, surface roughness and procedures such as doping technologies and front end process plasma etch etc.

Current status of the metrology tools with respect to the precision can be explained as follows: Scanning electron microscopy for critical dimensional metrology has proven precision of better than 1nm derived from the measurement of tens of thousands of identical structures. This provides the necessary control of the fabrication process. The accuracy of such a measurement is, however an entirely different issue and it is normal practice for different fabrication facilities making the same device to arbitrarily change absolute size data in order to make the various sets agreement with each other.

Thus measurement accuracy still needs improvement and more sophisticated hardware such as nano tip emitters, electron energy filters, monochromatic electron guns, aberration connected lenses, sophisticated electron optical columns and software such as automatic controls for optimizing and monitoring are viewed as keys for progress [13]. Contamination and charging of the sample are commonly existing issues in SEM that needs to be rectified [13]. This thesis however will show that what is generally the single largest and most common error 'distortion' in mapping action of the SEM has by contrast overlooked. Only when this factor has been corrected will the other problem become worth further attention.

Similar problems are found for the atomic force microscope (AFM) introduced more than a decade back to critical dimension measurement by Martin and Wickramasinghe at IBM [13].

The CD-AFM has a significant use in the measurement of line edge roughness, properties of edges and sidewalls of the structures; it also extends its support to CD SEM metrology as a tool matching reference. Traceable standards for CD AFM have been developed by collaboration of NIST and SEMATECH; these traceable standards influence the accuracy in measurement of the pitch and height using AFM [13]. The standard measurement uncertainties of CD-AFM are measured to be as low as 0.2% in measurement of step height of few hundreds of nanometers. The reduction of the tip width calibration with new probe technology and with the development of single crystal critical dimension reference materials (SCCDRMs) has resulted in accurate measurement with 1nm standard uncertainty [13].

In summary, though there are new technologies in the semiconductor metrology, SEM is remains the most widely employed, versatile and convenient tool for this purpose. The reasons for prominence of SEM in semiconductor industry are user friendly, high spatial resolution, highly automated operation, flexibility, and extensibility. In the next section various developments in SEM regarding technology and investigations carried out using SEM for metrology will be discussed.

2.2 CD SEM for metrology and errors in image based metrology

Scanning electron microscope is categorized as a specialized tool for the CD measurements in semiconductor industry and this section will deal with various parameters of the instrument that affect the measurement capabilities, discuss calibration methods and describe experiments performed to improve the performance of the CD SEM for feature sizes ranging from the micro-meter to the nano-meter range.

The operational parameters of the SEM that influence the resolution and measurement performance above are its beam energy, beam current, spot size and scan speed and these choices interact with each other in a complex way. The usual choice of the operating conditions for a SEM performing metrology is low beam energy (typically 200ev to 2kev) to reduce specimen charging and damage. Unfortunately this inevitably leads to poor source brightness, unsatisfactory signal to noise ratios and degraded electron-optical performance [10]. Because the signal to noise ratio falls with the beam current, a smaller beam spot size, while offering better image resolution and precision of the measurement and lower rates of damage and charging, worsens the signal to noise ratio and making it necessary to spend a longer time observing each feature of interest. Since most semiconductor materials do charge in an electron beam, charge control is an essential step to effective metrology. High scan speeds can provide one of stabilizing charging but adversely affects the signal to noise ratios and it will be shown later in this thesis that residual surface potential associated with this method can lead to large systematic errors in feature size measurements. An alternative way to control charging is the technique of Environmental Scanning Microscope (ESEM) which places the sample in a low vacuum (~100 Pa) environment. This is highly effective but requires the use of high beam energies which can lead to radiolysis and etching of resists and organic films.

Calibration of an instrument is the determination of any variation between the mean value of that instrument and the reference. Imaging capabilities of every instrument vary with feature structure and dimensions. Any slight change in the feature parameters like wall angle, edge roughness, surface roughness, will affect the precision and accuracy of the metrology. To obtain the desired accuracy of measurement, many techniques and experiments have been investigated [15]. Fabrication of reference standard for each and every feature can provide calibration for that

particular type, but fabrication of a standard for each structure would be highly impossible. Hence matching of the sample measurements from tool to tool is one of the solutions to maintain the accuracy and repeatability. A Comparison of measurements from CD SEM and CD AFM is one valuable methodology to reduce the possible uncertainty [15]. The line width measurement from three CD SEMs and CD AFMs used as reference are plotted against each other as shown below in Figure 2. Two of the SEMs are from same vendor, vendor A and third one is from vendor B. vendor A model 1 is the oldest of all the three SEMs used and vendor A model 2 is slightly different model and newer version compared to model 1. CD SEM from Vendor B is the newest model of all the three SEMs used [15]. It can be observed that the measurements from three tools have offset between each other from the 50nm line width to 250nm line width. It implies that same tools i.e., CD SEM with different hardware configuration or even same hardware configurations give different results, which are comparable to results from different tool such as CD AFM.

The main objective of this comparison is to show that the matching of measurement results from different tools would reduce the possible uncertainty than the matching of measurements results from same kind of tools. The reason why the results of the same type of tools give different results is due to their dependence on operational parameters of SEM such as beam spot size, signal to noise ratio, resolution and sample properties [15].

It is often suggested that the performance of SEM imaging tools can be effectively monitored by imaging samples such as gold or gold palladium coating on a carbon substrate and then measuring the smallest objects or the smallest spacing between the objects that can be discerned [16]. Using this methodology, the results obtained are totally sample dependent and resolution is not properly determined.

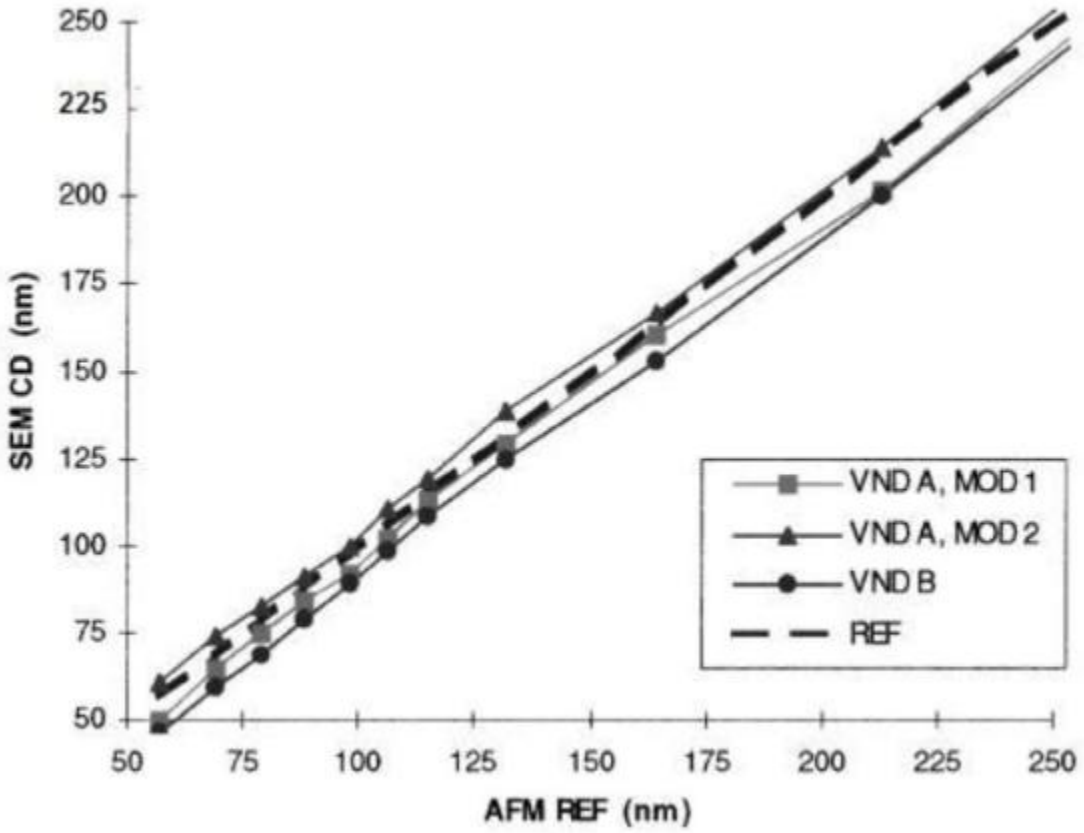

Figure 2: comparison of line width measurement from three CD SEM and a CD AFM [15].

Hence this method will misinterpret the general performance of the instrument. Reliable and meaningful measurement of resolution can be obtained by two dimensional Fast Fourier transform (FFT) of image to obtain power spectrum, or diffractogram [16]. Fast Fourier transformation of the images can be computed for example by applying well known public domain software such as 'NIH image' (for the Macintosh) or 'SCION image' (for Windows). In either case the program display the spatial frequency content of the image as distributed with increasing frequency radially from the center of the transformed power spectrum. Invariably the signal intensity is highest in the center of the display (which corresponds to the lowest spatial frequencies, i.e., the largest objects in the image) and falls as it moves away from center, eventually merging into the noise background of the microscope. The 'resolution' limit of the SEM then is reliably defined as the highest spatial frequency at which the signal is still distinguishable from the noise.

If the microscope is properly aligned and then electron beam is correctly stigmated then the FFT is supposed to be accurately circular, i.e., the spatial resolution will be the same in a direction in the image [16]. Obtaining the quantitative data from the power spectrum computed using NIH image or SCION image is made easier by using a specially written 'macro' sub-routine for these programs called as SMART (Scanning Microscope Analysis and Resolution Testing). This FFT based approach guarantees reliable information on resolution, accuracy of stigmation, signal to noise ratio and other parameters of the SEM, so providing significant improvement in the characterization of the measurement tool [16].

Another technique introduced to evaluate the accuracy and precision in critical dimension measurement of CD SEM is to compare the experimental results with results obtained from

Monte Carlo simulation of the interaction of electrons on the sample under similar experimental conditions. The CD bias is the difference between the measured critical dimension values from inline metrology tools and off line metrology tools and is most important factor to maintain the accuracy of the measurement of device structure measurements. The probable bias between the CD SEM and the reference tool data has been evaluated by using electron simulations which even consider the effects of the sample charging beneath the beam [17]. Thus, the pitch dependence of secondary electron signals profiles that is caused by charging leads to a systematic variation in CD bias values. Simulation results and experimental results showed good agreement for 300nm pitch structures but showed large deviations in the CD bias when compared for 80 nm pitch [17].

Such simulations are usually based on model libraries representing the expected geometrical parameters of the sample of interest. Monte Carlo simulations such as those for the secondary electron yields profiles at edges which are critical for measurement in SEM are complex program which run slowly and so cannot be directly used in measuring process. Signal profile are therefore pre-computed for a range of parameters and stored in a library [18]. Number of these libraries are then recalled with different parameter sets and compared against experimental profile to confirm the actual geometry encountered. The accuracy and repeatability of measurements of model based library and SEM are compared to monitor the performance of both the techniques. It is seen from the comparison that, during the top down imaging using SEM, there is repositioning of the lines from the edge and it is difficult to accurately identify that position. The edge bloom effect (bloom is the extra brightness on the edges compared to brightness on the pattern away from the edges) on the cross sectional image in SEM requires modeling under conditions corresponding to the same top down technique. Studies using the

model based library approach have also revealed other source of error such as the apparent dependence of the pattern geometry on the optical depth of field of the electron beam [18].

2.3 Moiré Metrology

The use of moiré fringe (from the French moiré – *mashed*) as a tool to characterize and correct SEM based CD metrology is a new concept although moiré methods have been employed for various other techniques such as scanning tunneling (STM) and atomic force microscopy (AFM). Moiré fringes are frequently when generated using electron beam imaging, but they have not previously been used for characterizing and calibrating SEMs.

Moiré fringes generated by the superposition of two grid patterns were first noted by Lord Rayleigh over 100 years ago. In general, when two periodic structures of similar frequency are superimposed on each other then an interference pattern 'the moiré fringes – with a new repeat frequency' is produced. Fringes are most clearly observed, when the two patterns are almost parallel and of equal spatial frequency, or when their periodicities have a simple harmonic relationship with each other. Moiré interference between other two dimensional features like circular zone plates are also well known and have been studied by many researchers. Because small displacements of either structure lead to large changes in the moiré pattern the fringes has long been applied to enhance the sensitivity of stress and strain analysis for a long time [19].

Many approaches have been proposed to explain the moiré effect, but Fourier transforms the most complete and convenient mathematical description. In the Fourier transform of two periodic structures interacting to generate moiré fringes, several strong peaks are observed. These correspond to the fundamental frequencies f1 and f2 of the structure themselves, and to one or more additional frequencies corresponding to the interferences between the f1 and f2

structures. The magnitude, position in Fourier space, and number of the beat components will depend on the fundamental periodicities of the parent structures and their orientation relative to each other. The parameters that can be obtained from the Fourier transform are the spatial frequency, orientation, and the profile of the pattern structure. The modulus of the vector that bridges the center of the transformed image and other strong peaks in the image define the spatial frequency of the pattern structure. The transformed pattern is computed by the performing convolution the two individual patterns. Convolution is the vectorial addition of the vector function of each individual pattern.

In general, the superposition of any two grating patterns will generate moiré effects. It is not however necessary for both structures to be same material in nature. Thus, when viewing a periodic object in a scanning electron microscope, moiré fringes can be observed as the results of interference between the physical periodicity of the object itself and the virtual periodicity of the scan raster. It is this effect which is exploited in the work in this thesis.

The moiré fringe produced by superimposing two straight line grating of the same frequency but positioned at a some angle to each other will be discussed further to explain the technique more thoroughly. In figure 3 (a), the straight line grating with equal frequency is superimposing of same line grating at an angle of 2α, resulting in moiré fringe pattern as in figure 3 (b). Dark fringe occur due to misalignment of one dark line over the other dark line by one and half period. These dark fringes are destructive interference of the line gratings. Similarly, bright fringes will occur due lo exact overlap of one dark line over the other dark line. These Bright fringes are constructive interference of the line gratings.

General representation of optical moiré pattern can be calculated by following Eq 1-3 [20]. Where the intensity transformation of each grating is defined as $f_1(x, y)$ and $f_2(x, y)$ and the

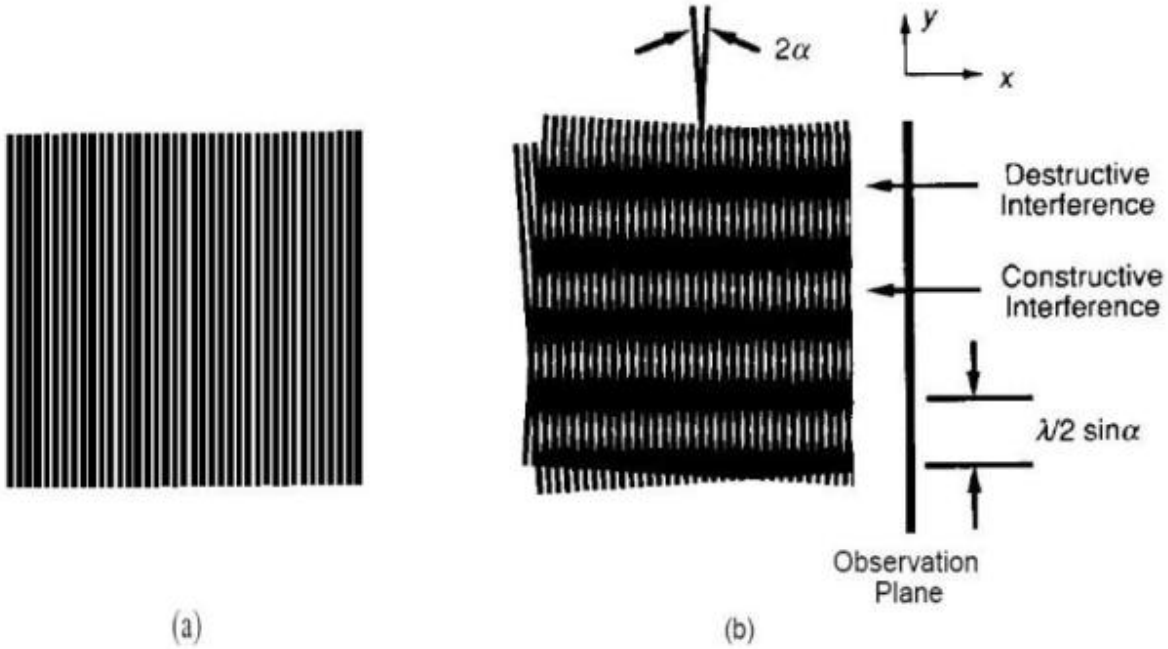

Figure 3: a) Straight line grating with equal periodicity b) moiré fringes formation by superimpose of straight line grating at an angle of 2α [20].

basic shape of the gratings is defined as Φ_1 (x, y). The moiré pattern intensity obtained by superimposing the two intensities f_1 and f_2 is given by the product [20].

$$f_1(x,y) = a_1 + \sum_{n=1}^{\infty} b_{1n} \cos[n\phi_1(x,y)] \quad (1)$$

$$f_2(x,y) = a_2 + \sum_{m=1}^{\infty} b_{2m} \cos[m\phi_2(x,y)] \quad (2)$$

$$f_1(x,y) \times f2(x,y) = a_1 a_2 + a_1 \sum_{m=1}^{\infty} b_{2m} \cos[m\phi_2(x,y)] + a_2 \sum_{n=1}^{\infty} b_{1n} \cos[n\phi_1(x,y)]$$

$$+ \sum_{m=1}^{\infty} \sum_{n=1}^{\infty} b_{1n} b_{2m} \cos[n\phi_1(x,y)] \cos[m\phi_2(x,y)] \quad (3)$$

In Eq 3, the properties of each individual pattern are given by first three terms. The last term gives the specific properties of the moiré pattern formed by superimpose of the two straight line grating patterns. The moiré intensity given by the Eq 3 can be further elaborated showing that the moiré pattern is caused due to addition and subtraction of dark line gratings [20]. The intensity in electron beam moiré in the SEM can be calculated similarly as Fourier product of the scattering power of the specimen grating and intensity scanning lines shown in Eq 4-8 [21]. Moiré fringe pattern formed by controlling the controls on the SEM can be classified as natural moiré fringes, fringes of multiplication and fringes of division. The raster scan pitch, scan line pitch and specimen grating parameters are considered responsible for creation of different moiré patterns [21]. The Moiré pattern formed by straight line gratings with a small angle tilt and no tilt for same frequency and different frequency are shown in Figure 4 [20]. Here the moiré patterns formed with different frequency and no tilt have been employed to explain the mapping errors of the SEM display and to propose some methods to over come the errors.

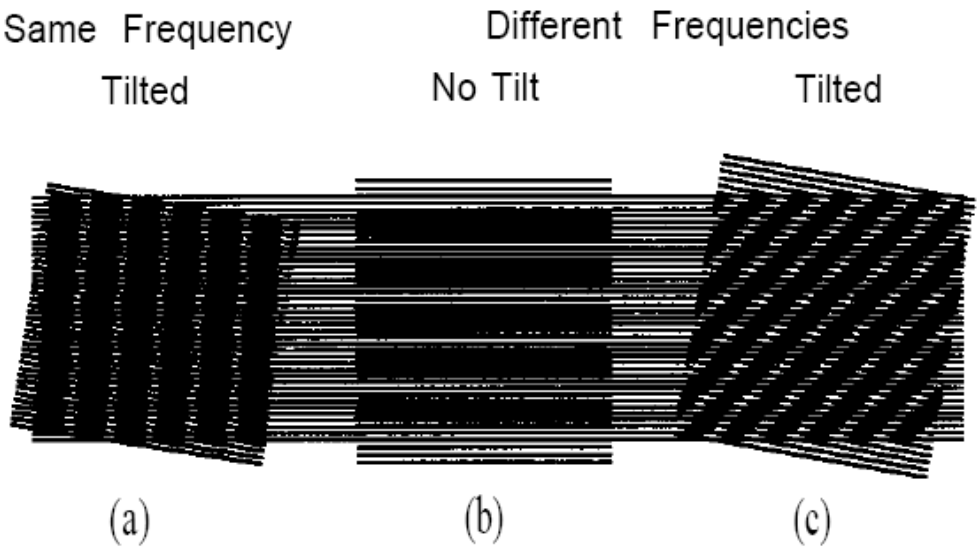

Figure 4: Moiré pattern formed by same frequency line grating and different frequency with tilt and no tilt along Y-axis [20].

2.4 Fourier representation of the moiré patterns by electron beam

The intensity of line grating G (y), is given by

$$G(y) = \frac{g_0}{2} + \sum_{n=1}^{\infty} g_n \cos(2\pi n f_g y) \tag{4}$$

Similarly, intensity of the scanning lines, *B(y)* is given by

$$B(y) = \frac{b_0}{2} + \sum_{m=1}^{\infty} b_m \cos(2\pi m f_b y) \tag{5}$$

Moiré fringe intensity, *I(y)* is given by product of *G(y)* and *B(y)* and this can be expressed as follows: $I(y) = B(y) \times G(y)$ (6)

$$I(y) = C + F(y) + S(y) + D(y) \tag{7}$$

$$I(y) = \begin{aligned} &\frac{g_0 b_0}{4} + \left(\frac{b_0}{2}\right)\sum_{n=1}^{\infty} g_n \cos(2\pi n f_g y) + \left(\frac{g_0}{2}\right)\sum_{n=1}^{\infty} b_m \cos(2\pi m f_b y) \\ &+ \sum_{m=1}^{\infty}\sum_{n=1}^{\infty} \frac{g_n b_m}{4} \cos 2\pi (n f_g + m f_b) y + \sum_{m=1}^{\infty}\sum_{n=1}^{\infty} \frac{g_n b_m}{4} \cos 2\pi (n f_g - m f_b) y \end{aligned} \tag{8}$$

$$f_g = f_g' \cos(\theta) = \cos(\theta)/ p_g' \tag{9}$$

Where g_0 = Fourier Coefficient b_0 = Fourier Coefficient

g_n = Fourier Coefficient b_m = Fourier Coefficient

p_g' = Physical grating of the pitch f_g' = Spatial frequency of the specimen grating

f_b = Frequency of raster scan lines

The Moiré intensity, *I(y)* represented by Eq. 8 is similar to the Fourier transformed equation for the moiré pattern in optical interferometry. The first three terms of Eq. 8 exhibit the frequency region of the pattern which is difficult to observe. The last part of the equation exhibits the moiré fringe pattern of the image [21].

Moiré pattern in SEM is observed due to interference of the raster scan line and the periodic structure of the sample. The periodicity of the sample cannot be changed but the periodicity of the beam can be changed by varying the field of view and the number of raster scan lines [22]. The mismatch of the raster scan and the periodic structure of the sample can be classified as the natural moiré fringes, moiré fringes due to rotation, moiré fringes of multiplication and fringes of division [21]. Figure 5 through Figure 11 are used to explain different kinds of moiré fringes formed due to raster scan mismatch.

Natural moiré fringes formation most obviously takes place, when the frequency of the specimen grating and the frequency of the raster scan are almost equal; this is called as near match condition. The natural moiré fringe pattern of specimen grating pitch of 200nm at 850X magnification is shown in Figure 5 and Figure 6 [21]. Moiré fringes due to rotation are mostly observed in optical moiré methods. The specimen grating and reference grating are held closely with small angle rotation in one of the gratings. Similarly moiré fringes due to rotation can be observed in electron moiré method. A Model of the fringes of rotation is shown in Figure 7, which explains the formation of the fringe pattern [21]. Moiré 'fringes of multiplication' occur when the frequency of the reference grating is almost equal to multiple of the frequency of the specimen grating. 'Fringes of division' occur when the specimen grating frequency is the multiple of the frequency of the reference grating. Figure 8 through Figure 11 exhibit the fringes of multiplication and fringes of division for 200nm specimen grating at different magnifications. The notation developed for fringes of multiplication, fringes of division and fringes of rotation in optical moiré can conveniently also be used to represent the respective fringe pattern in electron beam moiré method [21]. SEM moiré fringes pattern disappear at a specific magnification called as null magnification and the corresponding conditions are called null moiré condition.

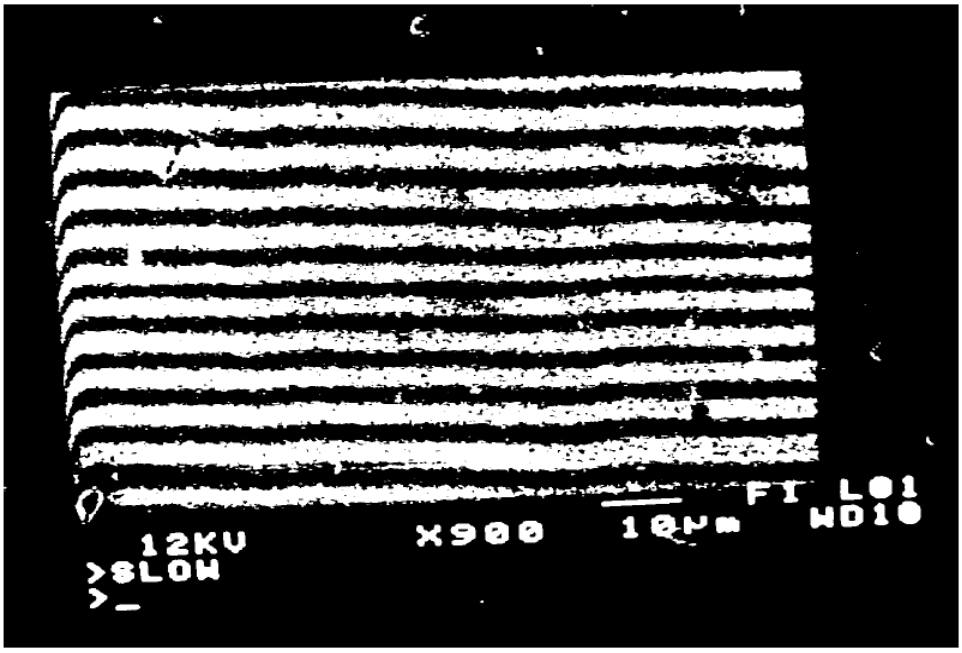

Figure 5: Natural moiré fringe pattern for grating pitch = 200nm at 900X magnification [21]

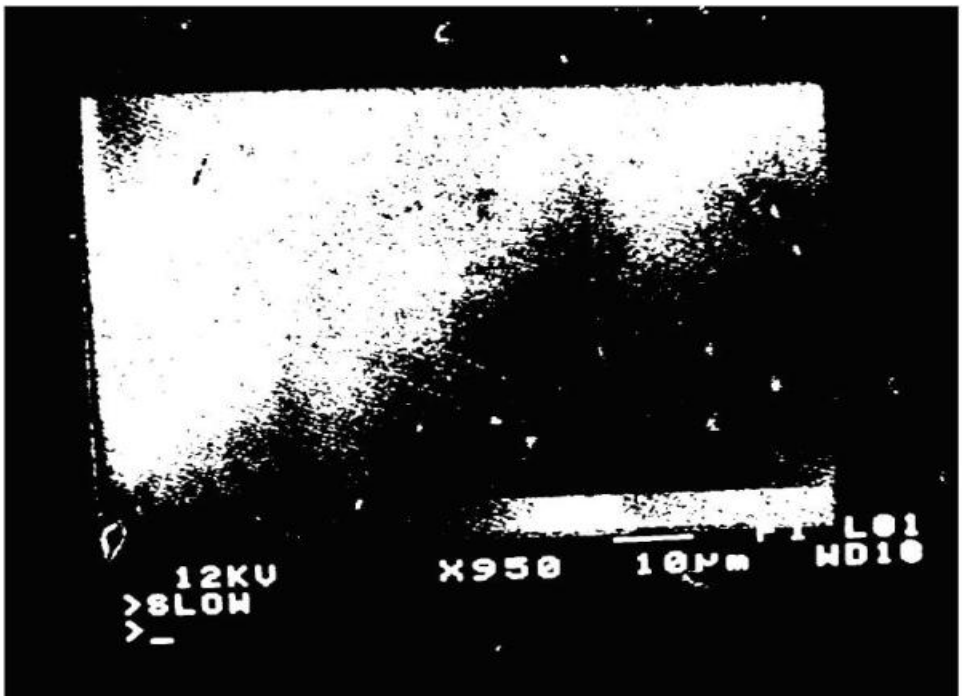

Figure 6 : Natural moiré fringe pattern for grating pitch = 200nm at 950X magnification, perfect mismatch exhibits no mismatch at all [21]

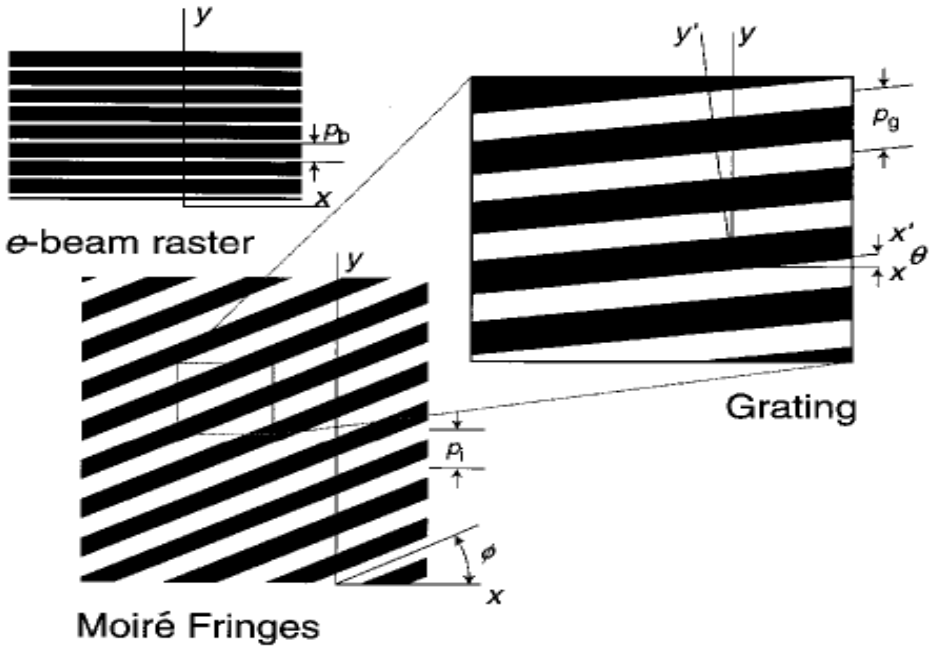

Figure 7: Model of Moiré fringe pattern due to rotation of one of the grating by a small angle [23]

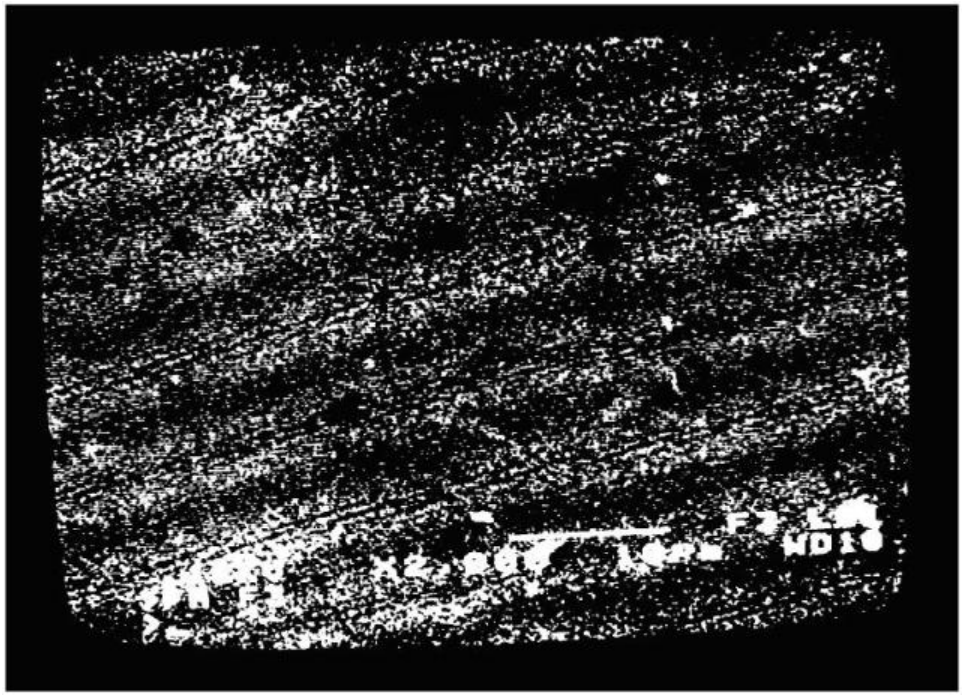

Figure 8: Fringes of multiplication for 200nm line grating pitch at magnification of 2000X [21]

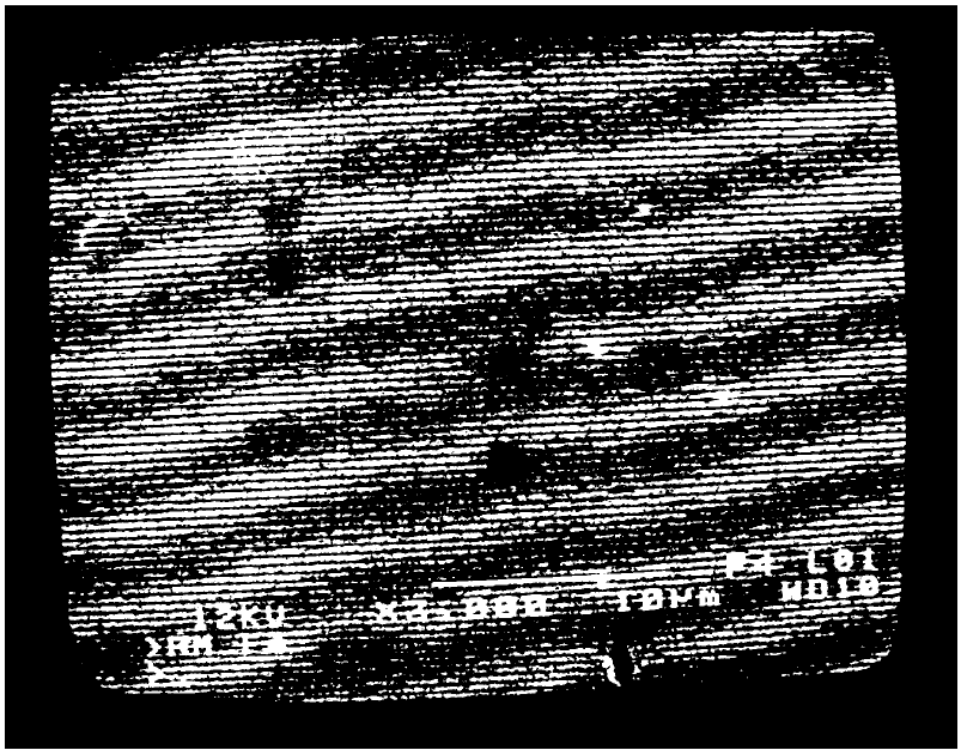

Figure 9: Fringes of multiplication for 200nm line grating at magnification of 3000X [21]

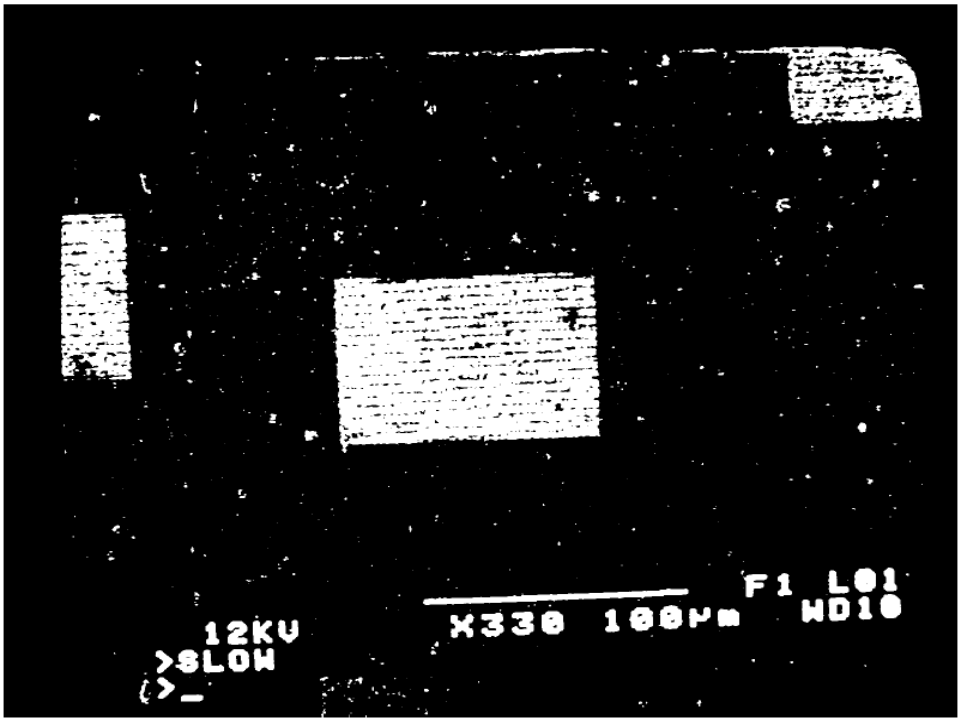

Figure 10: Fringes of division for 200nm line grating at magnification of 330X [21]

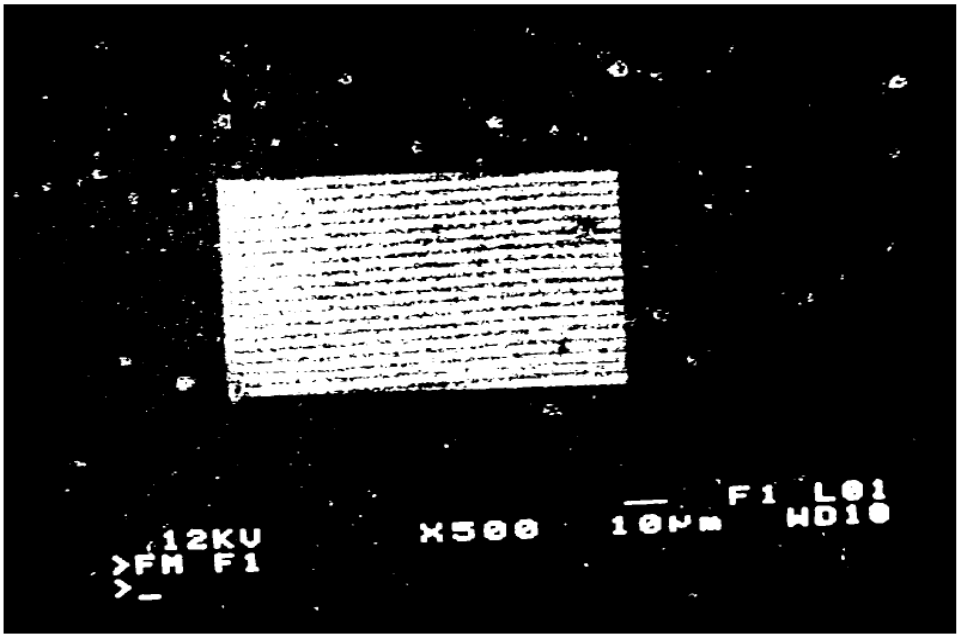

Figure 11: Fringes of division for 200nm line grating at magnification of 500X [21]

The null magnification is dependent on the spatial frequency of the specimen grating and on a factor given by the Y-axis dimension of display divided by the number raster scan lines explained in Eq 10 [21].

$$M_n = \frac{S}{R} \times f_g \qquad (10)$$

Where M_n= null magnification

S =Y-axis dimension of the display

R =Number of raster scan lines

f_g= Frequency of the specimen grating

The null magnification value can be identified by calculating the Eq 10 with known value of the specimen grating frequency, the display dimension in Y –axis and the number of raster scan lines. In order to achieve the null moiré condition, the field of view has to be carefully adjusted by changing the magnification. Because changing the magnification by the varying the working distance (WD) of the SEM is will also be necessary to apply the raster rotate control to ensure that the raster scan lines remain exactly parallel to specimen grating lines [22]. The true magnification of an SEM image is likely to be different from the indicated magnification on the viewing screen. Once a null magnification value has been established for a given set of operating conditions then the electron beam moiré can be used to provide an absolute calibration the magnification of the SEM. The resolution and sensitivity of the measurement made by the electron beam moiré method are controlled by the specimen grating frequency. Fringes of division and natural fringes can be identified easily, where as fringes of multiplication need high contrast line grating fabricated on the sample in order to enhance the sensitivity of the fringe pattern. Fringes of division are observed at low magnifications and hence exhibit higher order of

Fourier coefficients and field of view. While the sensitivity of each fringe in natural moiré pattern are maintained unchanged, the lager field of view can be observed through fringes of division. Calibration of SEM at each unique magnification is necessary to maintain the accuracy and repeatability of the machine. Characterizing the performance of SEM can be achieved from the electron beam moiré fringe mismatch for each magnification [21].

In the present work, moiré techniques are used for calibrating and identifying the mapping errors in the display scanning electron microscope.

CHAPTER 3

EXPERIMENTAL PROCEDURES

In this present work high precision patterns of various geometries fabricated on to a silicon wafer were imaged in a CD SEM to demonstrate how it is possible to identify the errors in the raster of the SEM such as X and Y scan non-linearity and lack of orthogonality. Moiré patterns derived from the wafer were also used to check the magnification calibration of the SEM. This chapter describes the sample used for calibrating the SEM and the special features of the SEM used in the work are described. Also the operating procedure for the SEM is explained in detail.

3.1 Sample description

A silicon wafer sample containing a wide variety of line grating features was used to calibrate the magnification, and to identify the mapping errors in the SEM. This sample was designed for applications in the fields of critical dimension and overlay metrology fabricated by Metro boost Inc, Santa Clara, CA. This sample is a poly crystalline silicon wafer covered with a thin layer of oxide of about 2.5 to 3nm on the surface. Metro boost fabricates and certifies these samples as calibration standards for the SEM and other metrology tools such as the scatterometry.

The 20mm by 20mm silicon wafer contains patterns written in 16 blocks of 5mm each side. These structures are first fabricated on a mask and then later transferred to the silicon wafer through optical lithography. The features on the mask at the smallest pitch do not usually show up on the wafer due to resolution limitations of the fabrication process [24]. Features with

pitches from .25 μm, .26μm and above are guaranteed for their dimensional accuracy and visibility [24]. These features are utilized for experimental purposes The most clearly visible features are those with a pitch above 5μm, therefore the features utilized in the present work are range from 5μm to 30μm. There are over 1000 features in the sample wafer but it is the circular disks decorated with line gratings that are utilized here to calibrate the magnification and to identify mapping errors by using moiré fringes formed by the interference between the raster scan and the line gratings on the sample. Though moiré fringes can be easily observed in any line grating features, the circular disk features are preferred because shape distortions can be more easily identified at various magnifications.

3.2 Working of SEM

The SEM shown in Figure 12, is the S4300 manufactured by Hitachi (Hitachi High Technologies, Pleasanton, CA), and was used to perform all the experiments in the present work. The special features of SEM 4300 include variable pressure technology (1 to 300pa) and a Schottky electron gun. These features allow high resolution imaging for all types of insulating materials, while operating it at variable pressures. The Schottky gun in the SEM enhances the resolution by allowing the user to produce small probe sizes and high density current. The Schottky gun, the condenser and objective lenses, the choice of working distance, the objective aperture size, and probe diameter all play very important roles in determining the image resolution. The functioning of these components is explained in detail in the next section of this chapter followed by sample description, sample loading in specimen chamber and imaging.

Figure 12: Scanning Electron Microscope Hitachi S4300, Electron Microscopy Facility at University Tennessee Knoxville.

Field Emission gun: Field emission guns have several advantages over thermionic emission. Thermionic emission depends on temperature of the order of 3500^{o} to emit electrons from the cathode. This requirement results in several disadvantages such as limited life time of the cathode, low brightness (amps/cm^2/sterad), and a large, thermally induced, energy spread. Field emission (FE) sources, on the other hand, do not rely on temperature to excite the electrons from the cathode but rather on the tunneling of electrons resulting from very high electric fields at the emitting tip. Such emission tip is a wire with a point of radius less than 100nm, which is supported by a tungsten "hair pin". Tungsten is the most commonly used (tip) cathode material because of toughness and low cost, but carbon and silicon nano tubes have also been used successfully. When a negative potential is applied to the cathode, the electrons concentrate on the tip and work function barrier is lowered. When the field at the tip reaches a magnitude of about 10V/nm electrons can tunnel through the work function barrier. A Cathode current density of 10^5 A/cm^2 can be produced by field emission gun [25].

There are two types of field emission guns namely Cold field emission (CFE), Thermal field emission (TFE). Cold Field emission and thermal field emission share same properties with distinction that the TFE being operated at an elevated temperatures (1750K). A TFE gives enhanced results even at modest vacuum conditions as the high temperature keeps the tip clean, reduces noise and instability, where as in contrast the CFE needs to be flashed at least once for few hours to clean the tip and keep the emission current stable.

A Schottky emitter is actually a thermionic source whose brightness is enhanced by both applying a field to the tip and by flowing ZrO_2 over the tip to reduce its work function. In order to ensure that SFE tip is clean and stable, the gun is run continuously, even when no current is being drawn from it. The life time of SFE depends on presence of the deposited ZrO_2 layer and

typically the cathode needs to be changed every 12-15 months as compared with the CFE and TFE tips which last for many years [25]. However the Schottky emitter is highly stable, is always instantly available for use without the need to clean and form the tip, and provides higher beam currents than the field emission sources

Lenses in SEM: Condenser and Objective lenses are required in the SEM to demagnify the diameter of the electron beam. Typically two condenser lenses are required and the first and second lenses are coupled together to enable single control. Demagnification of the electron beam is controlled by the 'spot size' setting for various imaging modes. Objective lenses are stronger than condenser lenses that is to say that they have a shorted focal length, because their excitation (the current passing through their winding) is high. The objective lens also contains the beam scanning coils, the stigmator assembly, and the aperture which defines the convergence angle of the focused beam and is controlled by the "focus" setting [25].

All the lenses in the electron optics are aligned on to a common axis. The electron beam must lie on this axis if the image is to be observed with correct shape, size and position. If the lenses are not correctly aligned with the axis, then the images are stigmatic and cannot be focused properly. The ultimate imaging resolution of the microscope is limited by the aberrations of the objective lens. There are two main types of aberrations; Spherical and Chromatic. As a result of spherical aberrations electrons traveling at a large angle to the axis are brought to a focus at a different point to those traveling on axis. As a result of chromatic aberration electrons of low energy are brought to a focus closer to the lens than those of higher energy. Both aberrations degrade the resolution and distort the image [25].

Astigmation arises because the objective lens cannot be made to be perfectly cylindrically symmetrical about the beam axis. Contamination in the column and on the apertures can also

result in astigmatism. Because astigmatism severely limits image resolution a stigmator must be used to correct the astigmation. The stigmator, typically a hexa-pole or octo-pole device, applies an external weak magnetic field whose magnitude and direction can be adjusted as required to cancel the asymmetry of the lens [25].

Working Distance: The working distance (WD) of an SEM is the distance between the bottom of the objective lens and the top of the sample. The WD can affect the image resolution even without changing any other lenses or aperture. As the working distance increases, the object moves far away from the lenses and resulting in an increase in the spot size although the depth of field is improved. Large working distance can be used when low magnification imaging is required but shortest working distances are always preferable when a high resolution of the image is desired. In the present work, images with high resolution at high magnification are necessary hence smaller working distances(15mm and less) were used [25].

Aperture Size: The diameter of the final aperture in the objective lens controls important parameters such as the imaging aberrations, the final probe current and the depth of the field because the aperture size determines the convergence angle of the electron beam entering the final objective lenses. Reducing the aperture angle minimizes the aberrations in objective lenses and provides a smaller final probe size, but because the choice of aperture size strongly affects the final probe current, as only a small fraction of the beam current is allowed to pass when the aperture is small. In addition reducing the probe convergence angle of the electron beam increases the depth of field. Since the present work emphasizes more on the surface feature for sharp image contrast, a normal sized aperture is used [2512].

Probe Size: The Probe size, i.e. the diameter of the focused electron beam as it reaches the sample surface, mostly determines the image resolution. Smaller probe sizes give higher

image detail but at the expense of a reduced beam current and poorer signal to noise ratio. Larger probe sizes lead to poorer resolution but higher currents and improved signal to noise ratios. The appropriate choice will depend on the details to be observed at any time [25].

3.3 Experimental Procedure

Specimen Chamber: The specimen chamber in the SEM is where the sample is loaded in order to perform the experiments. The chamber is maintained at a vacuum of $7x10^{-4}$ Pa, in order to avoid contamination of the chamber, in high vacuum mode, but in low vacuum operation the pressure can be as high as 400Pa. Figures 13 through Figure 15 exhibit the specimen chamber and mouse controls. The sample is loaded on to a motor driven stage in the specimen chamber through a specimen exchange chamber Figure 13. The stage can be controlled by using a 'mouse' or by a specially designed stage control as shown is Figure 14. Manual controls of the stage are also located on the specimen chamber as shown in Figure 15. The stage can be moved in X, Y and Z directions and can also be rotated about its axis and tilted up to 60 degrees.

Loading the sample in specimen chamber: The silicon wafer to be viewed in the SEM is first cleaned thoroughly by blowing it with nitrogen gas to avoid contamination in the chamber due to dust on the sample. The sample is then mounted on to the specimen holder with double sided copper tape. The specimen holder is a fixture that carries the sample and is designed to hold itself perfectly on the specimen stage. Since the working distance depends on the height of the specimen holder, it is very important to check the height of specimen holder before loading the sample since if the height is too high, it may touch the lenses or if the height is too low, it may not be possible to achieve focus.

Once the specimen holder is loaded, the specimen exchange chamber has to be vented by pressing AIR on the SEM display screen in order open the viewing glass of the exchange chamber to load the sample on to the exchange rod in the viewing glass. After loading the sample on the rod, the VAC button is activated to attain the vacuum in the specimen exchange chamber and to permit the transfer of the sample on to the stage. Once the specimen exchange chamber is vacuum tight, the door to the specimen chamber can be opened allowing the specimen inside the chamber. The specimen holder is fixed tightly on the stage and the exchange rod is decoupled from the specimen allowing the closing of the specimen chamber door. It takes few minutes to attain the vacuum after the chamber door is closed.

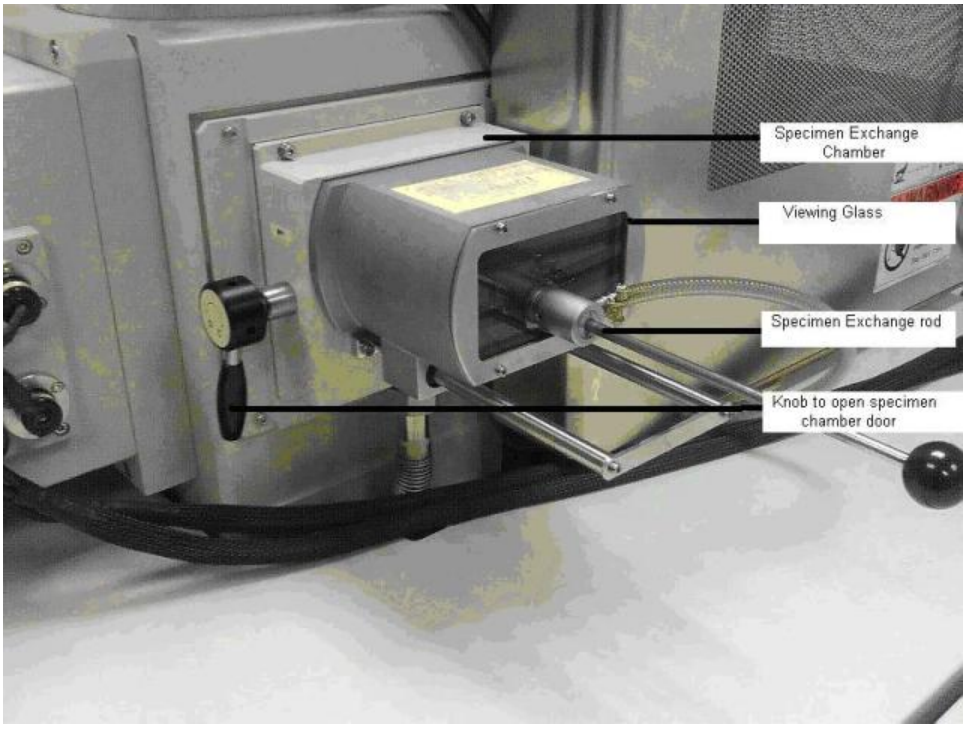

Figure 13: Specimen Exchange Chamber

Figure 14: Mouse control for stage in X and Y directions

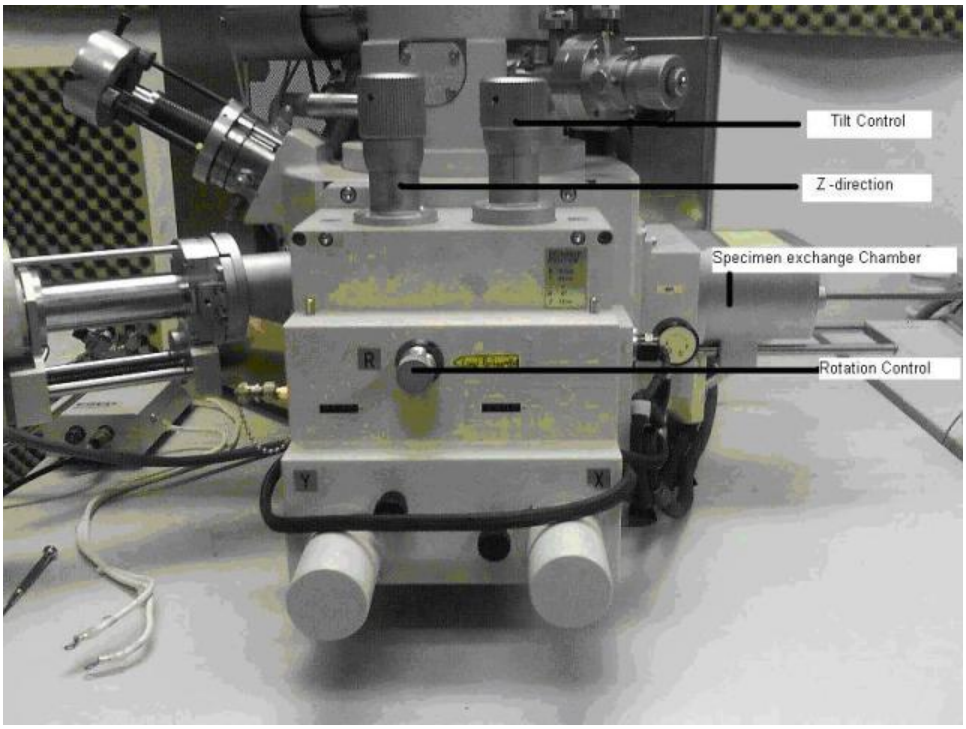

Figure 15: Specimen Chamber

The electron gun can be turned on only after making sure that the vacuum in the chamber is lower than about 10^{-3} PA

Imaging: Capturing a clear and sharp image needs some basic steps such as the correct alignment of beam, focusing the beam, appropriate selection of the OL aperture, and setting the X-stigmation and Y-stigmation controls. Once the image is visible the Brightness and Contrast controls need to be adjusted in order to increase the visibility of the image and to optimize its presentation on the screen. The working distance is chosen to achieve the best balance between image resolution and depth of field. Since high resolution images are required for the present work, and because wafer is flat and has little topographic detail a working distance of 5mm are usually selected as offering the best compromise between resolution and depth of field.

Images captured for the experimental work in this thesis were taken in various conditions and at many positions of the sample to investigate the following phenomena.

1. Moiré fringe behavior with the increase in magnification at constant working distance
2. Moiré fringe behavior with varying working distance at constant magnification
3. Non linearity of X and Y scan raster with moiré fringes
4. Orthogonality of the raster scan X and Y axis co-ordinates.
5. SEM center offset, Zoom center and stage center calibration

The images captured are analyzed and studied with help of power spectra i.e. Fast Fourier Transformation (FFT) computed using Image J software from Wayne Rasband, NIH, Washington DC [26]. . Results and analysis of these images will be discussed in next chapter.

CHAPTER 4

RESULTS AND DISCUSSIONS

This chapter demonstrates the results obtained from experiments performed to identify the mapping errors in the SEM. The sample used for experiments is designed for applications in the fields of critical dimension and overlay metrology, and is fabricated by MetroBoost Inc, (Santa Clara, CA 95051). This sample is a poly - crystalline silicon wafer with a layer of oxide (thickness of 2.5 to 3nm) on its surface. Metro Boost fabricates and certifies these samples as calibration standards for the SEM and other metrology tools such as the scatterometry.

In this study, the sensitivity of the moiré fringes with respect to various factors is utilized to identify the mapping errors in raster scan of the SEM. Moiré fringes observed here are formed by the mismatch of the line grating features in the sample and the raster scan lines (virtual scan lines). The hidden distortions in mapping process of the SEM, demonstrated in these sections is applicable to – and likely to be observed in - all other tools which use raster scanning technique for imaging and measurement purposes.

4.1 Moiré fringe behavior with the magnification

Multiple line grating patterns fabricated by MetroBoost are used to study moiré fringes, which are formed by due to the interference of raster scan lines with the grating patterns. The nature of the moiré fringes formed depends on the imaging magnification and the spacing of the raster scan lines. The spacing between the moiré fringe (d_m) patterns formed by the interference of raster scan line (with spacing d_1) and specimen line grating (with spacing d_2) can be calculated by equation (1).

$$d_m = \frac{1}{\left[\frac{1}{d_1} - \frac{1}{d_2}\right]} \qquad \textbf{(11)}$$

Figure 16 illustrates how the raster scan lines interfere with line gratings on the sample to produce moiré fringes. Figure 16(a) shows the pattern of the line grating in the specimen (d_2), similarly Figures 16(b), 16(c), and 16(d) show how the spacing changes in the raster scan line (d_1) with the magnification. Figures 16(e),16(f) and 16(g) show the corresponding moiré fringe pattern spacing (d_m) and Figures 16(h), 16(i), and 16(j) show the corresponding FFT of moiré fringe pattern.

In the illustration described above at lower magnifications the raster scan lines (d_1 is small) are very closely packed and the FFT corresponding to the moiré fringe formed at this condition is a power spectrum with two intensity points (Figure 16(h)). Moiré fringe spacing d_m at this condition is very small compared to those at higher magnification (Figure 16(j)). At certain magnifications, where the raster scan line spacing (Figure 16(c)) is almost equal to that of line pattern in specimen (Figure 16(a)), near matching condition will occur and simple moiré fringes will be formed. The FFT of moiré fringes of such condition is shown in the Figure 16(i). In Figure 16(d), raster scan lines shown are at a very high magnification; hence the fringe spacing formed at this condition is large compared at other magnifications. The FFT at this condition is as shown in figure 16(j).

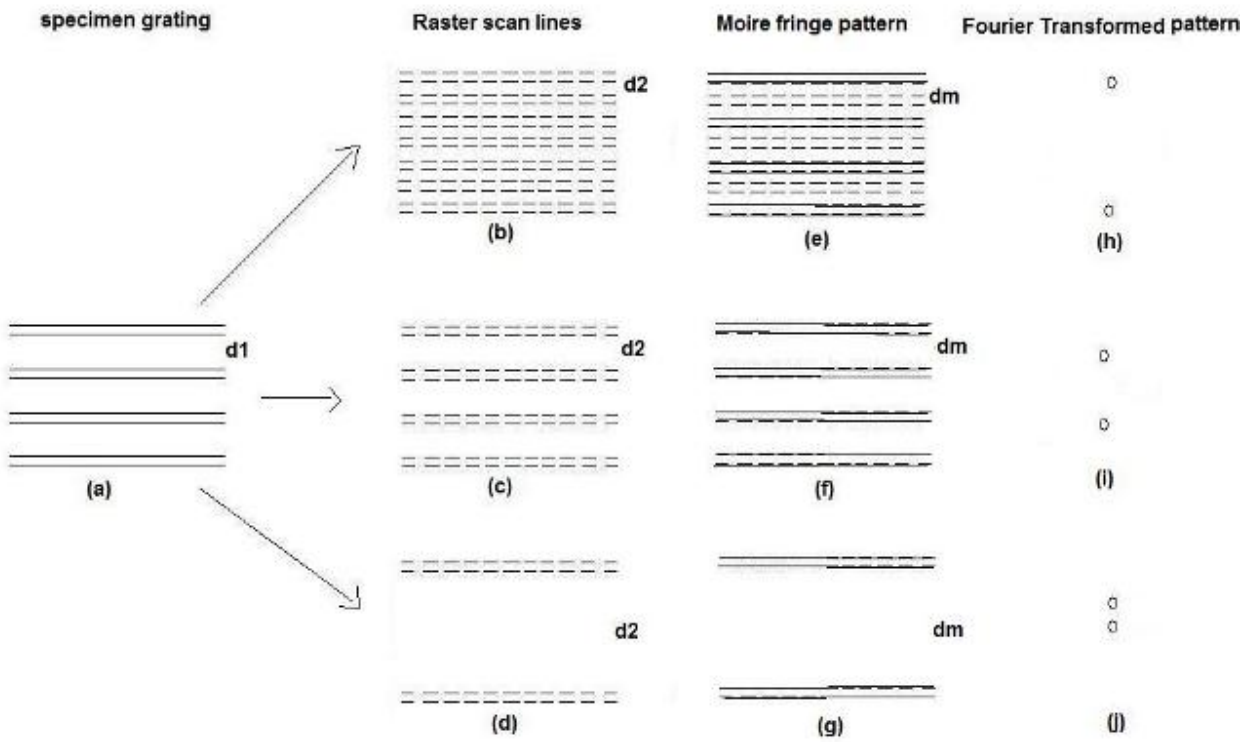

Figure 16: Model of interference of line grating on sample and raster scan lines, (a): the line gratings in sample, (b),(c) and (d): raster scan lines at various magnifications , (e),(f) and (g): Moiré fringe pattern, (h),(i) and (j): corresponding FFT for moiré fringes.

It can be demonstrated from the illustration that with the change in magnification from lower to higher values, the moiré fringe spacing increases, which lead to the maximum intensity points (power spectrum) in the FFT to come closer to each other. This behavior continues with the increase in magnification until, at a particular magnification, the spacing between the fringes tends to infinity and then loses visibility. This magnification can be referred to as null magnification M_n [21]. Here, it can be noted that the magnifications at which the similar moiré patterns are observed, occur at multiples of the lowest magnification at which the moiré pattern was first observed. Figures 17 through Figure 23 are examples of the moiré fringe patterns that are formed in the SEM on the line grating sample with the line pitch less than 0.5μm at values of magnification from 400X to 2.5KX. In Figure 17, the FFT of the line grating patterns observed at same range of magnifications as above.

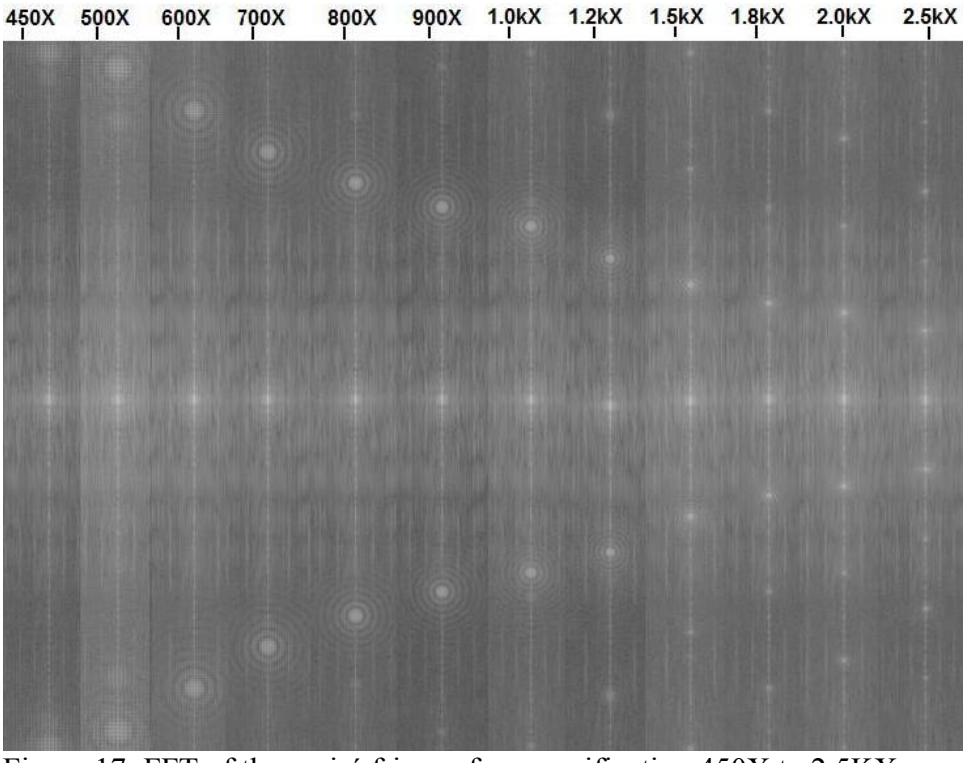

Figure 17: FFT of the moiré fringes for magnification 450X to 2.5KX

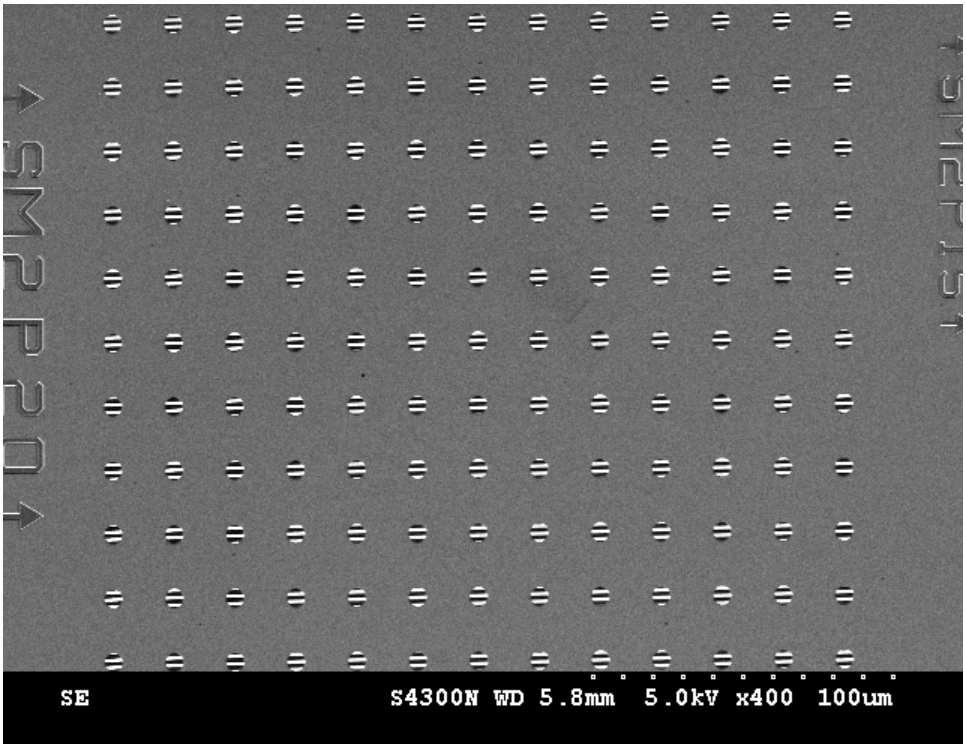

Figure 18: Moiré Fringes observed at magnification 400x

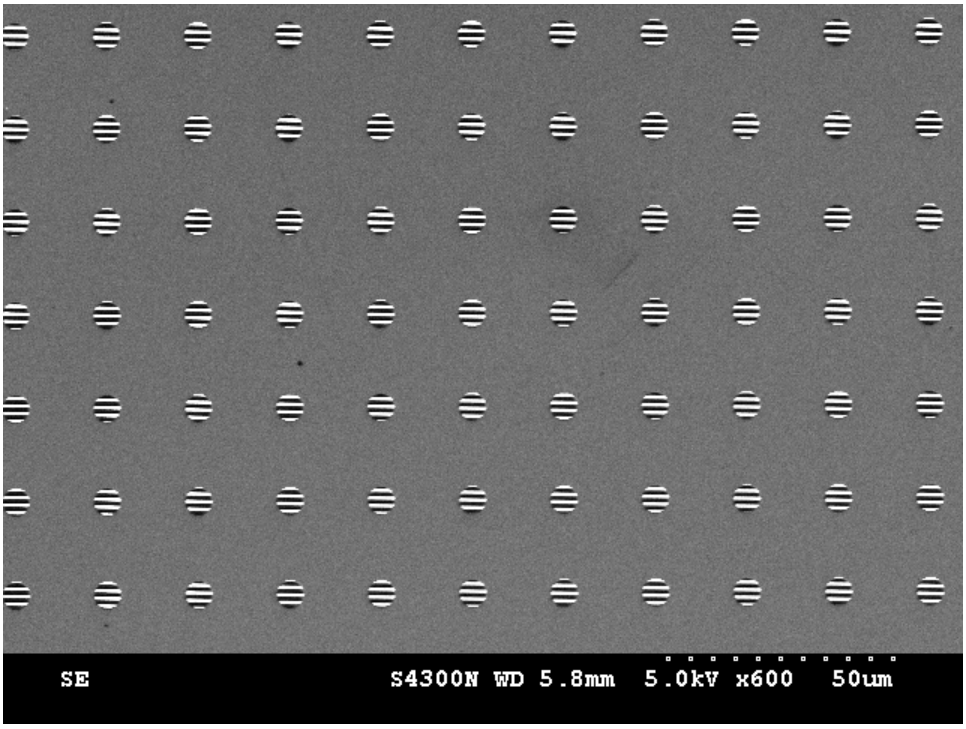

Figure 19: Moiré Fringes observed at magnification 600x

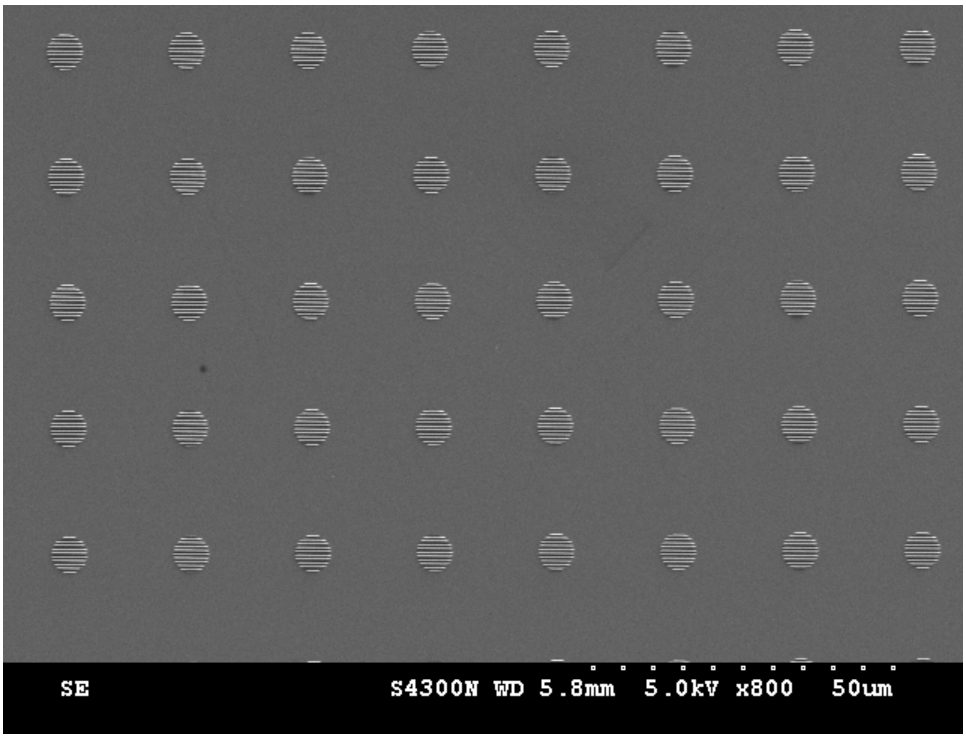

Figure 20: Moiré Fringes observed at magnification 800x

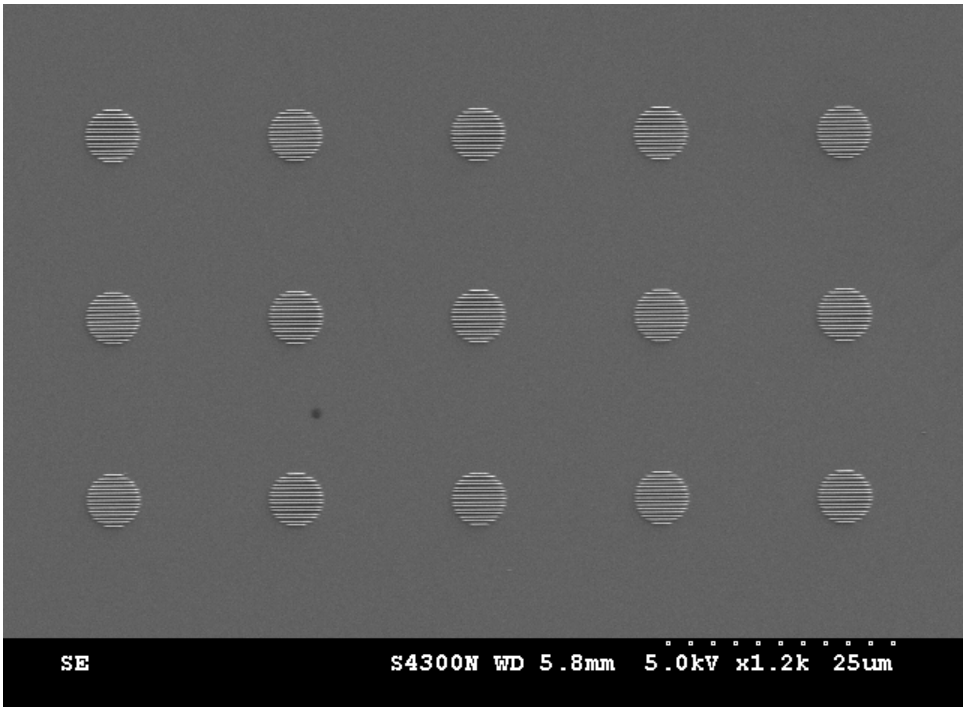

Figure 21: Moiré Fringes observed at magnification 1.2Kx

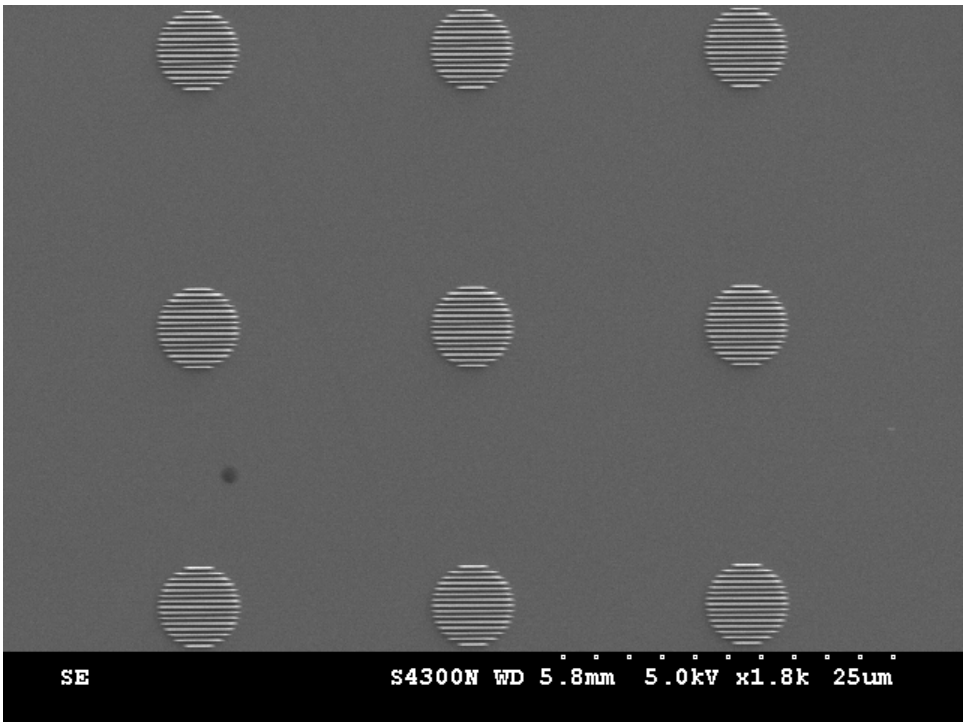

Figure 22: Moiré Fringes observed at magnification 1.8Kx

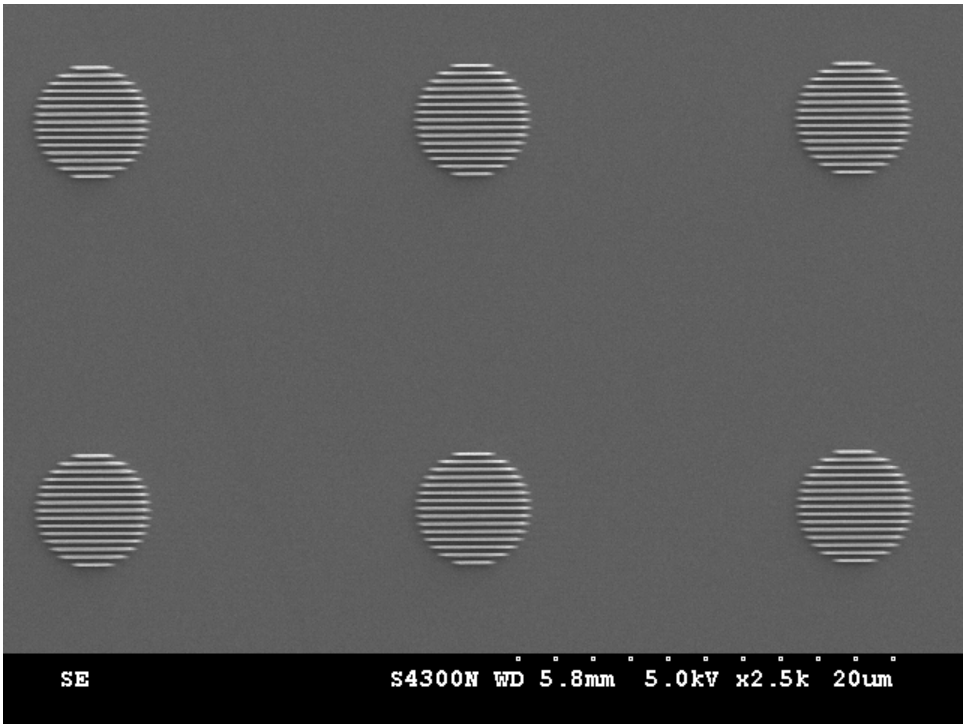

Figure 23: Moiré Fringes observed at magnification 2.5Kx

4.2 Moiré Fringe behavior with varying working distance at constant magnification

The interference fringes formed between the circular disk line grating and the raster scan lines are observed at various working distances in the SEM. When the working distance was increased, the focal length had to be changed and the objective lens adjusted so as to focus the specimen properly. During this adjustment there is possibility that the raster scan will change its orientation as a result of the rotation in the image which occurs because of the spiral trajectories traced by the electron beam as it passed through the magnetic lens field. This effect cannot be identified directly by viewing the image. The sensitivity of the moiré fringes is utilized here to observe and identify these effects. It can be seen in Figures 24 through Figure 27, how the moiré fringes are affected by varying the working distance. In Figure 24, the pattern in which the fringes repeat themselves as bands is exhibited to demonstrate the phenomena further clearly. This exact form of these effects changes with the working distance and there is slight variation in the orientation of the features; the pattern is used only to demonstrate that fringes formed in present experiments follow a similar analogy.

In Figures 25 to Figure 27, 20 μm pitch circular disks are observed at working distances of 5.8mm, 7.8mm and 9.9mm at magnification of 1.0Kx. A few degrees of rotation is noticed in the moiré fringes with increase in working distance from 5.8mm to 9.9mm. As shown in the illustration (Figure 24) of the moiré fringe pattern, it can be noticed in each of the Figures 25 through Figure 27 that the fringes repeat themselves in a specific manner at each chosen working distance. This implies that the change in working distance affects the resolution and magnification of the image and needs attention.

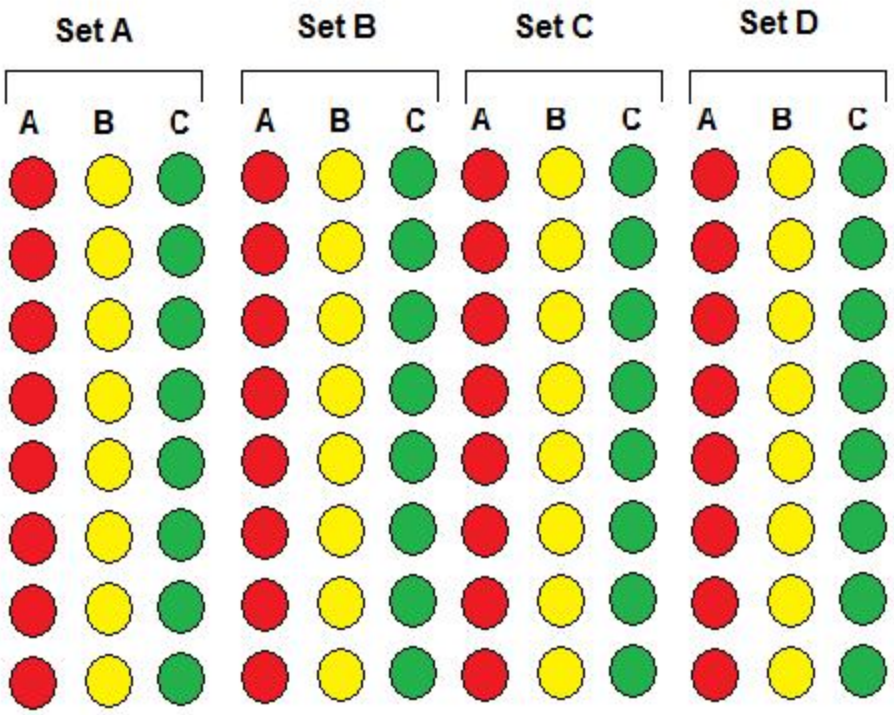

Figure 24: Model exhibiting the behavior of the moiré fringes

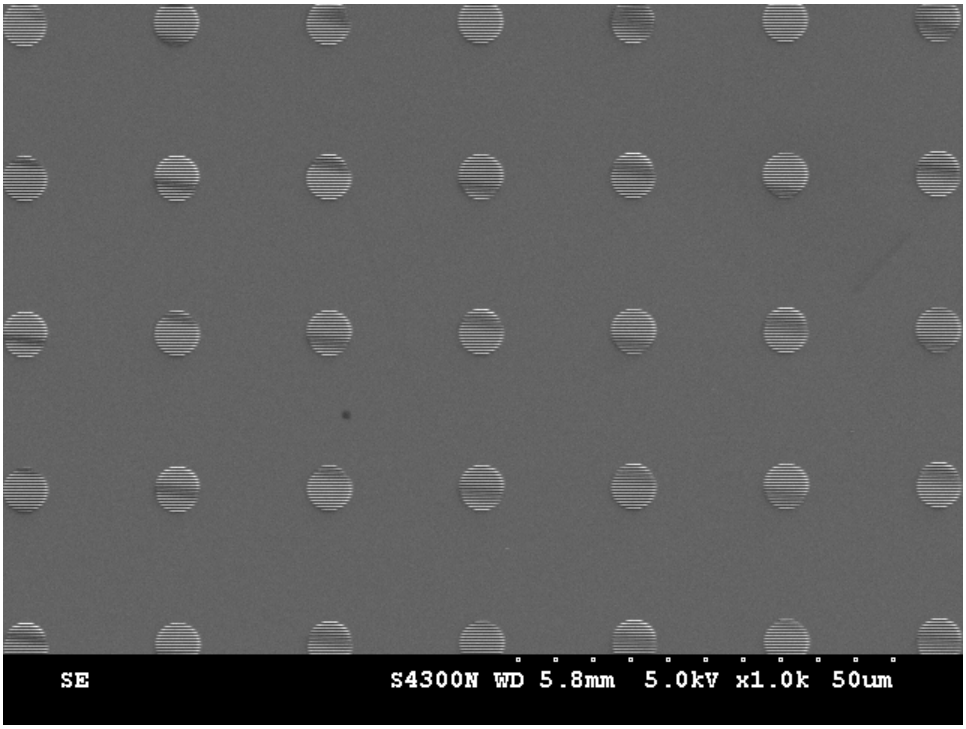

Figure 25: Moiré fringes formed at working distance 5.8mm

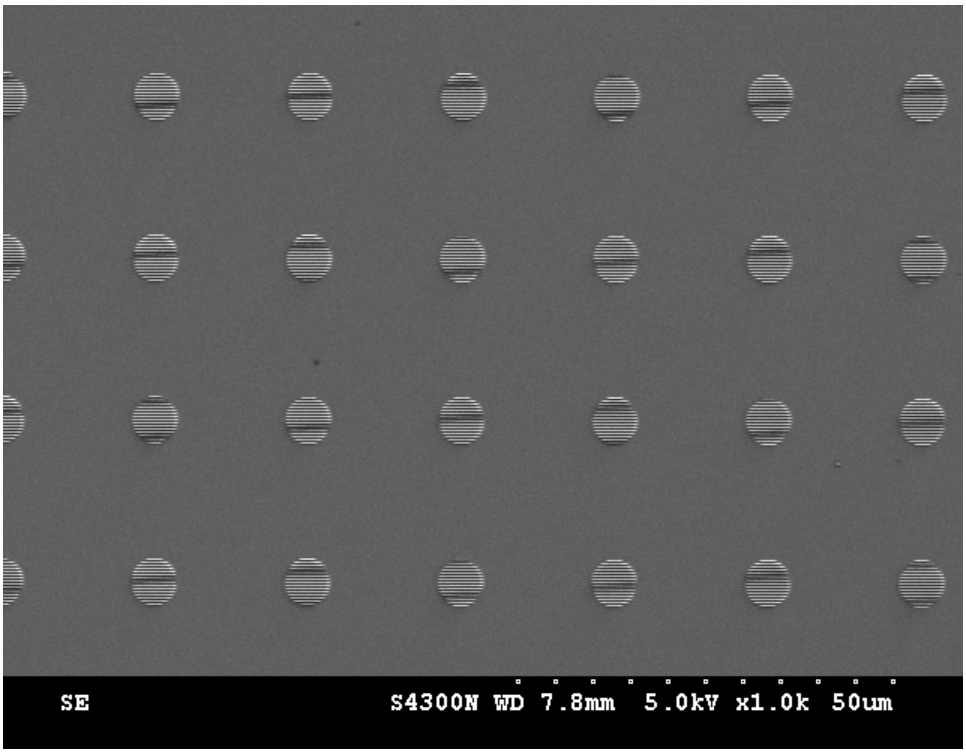

Figure 26: Moiré fringes formed at working distance 7.8mm

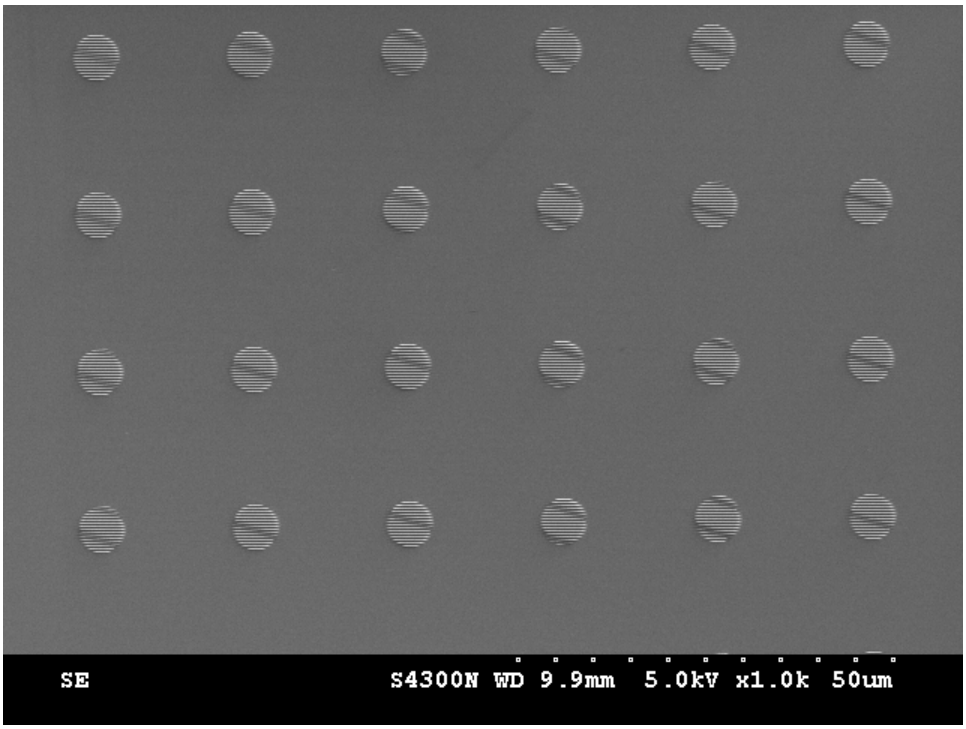

Figure 27: Moiré fringes formed at working distance 9.9mm

4.3 Moiré fringe's sensitivity for raster scan distortion

The non-linearity and non-orthogonality of the x and y axes are major concerns addressed by the results presented in this section. Moiré fringes can identify distortion which results from the raster scan line irregularity and non-linearity. Generally, the fringe formed by interference of the line grating and the scan lines are expected to be straight and parallel to the X and Y axes of the display screen. The pattern used to demonstrate what happens when non-linearity occurs is shown in an arrow shaped structure containing a line gratings array whose components are expected to be straight and parallel to the length of the arrow. The images showed in Figures 28 and Figure 29 exhibit moiré fringes which, clearly, are not parallel to the co-ordinate system. A straight white line drawn in Figure 14 is used to indicate the non linearity whose magnitude measured by Image J (from Wayne Rasband, NIH, Washington DC), is found to be approximately 6% along X-axis in both cases illustrated in Figure 28 and Figure 29.

There could be several reasons for this marked non-linearity in the raster motion. One possibility could be that the current in the orthogonal axes produced by two different circuits (i.e. the line and the frame directions). The current in the two circuits and the resultant deflections along the two scan axes cannot be always exactly same. Hence the difference in the deflection in the two orthogonal circuits is seen as non linearity. Another explanation is that the scan speed adversely affects the linearity of the raster scan. With the increasing scan speed there is possibility that the 'back EMF' generated by the inductance of the line scan coils in the SEM cannot be accommodated or corrected by the scan amplifier and so leads to a deflection of the beam scan point from its expected position. The non linearity in the raster scan can be reduced by observing the sample at longest possible working distance (to minimize the angle through which the beam needs to be deflected) and capturing the image at slowest scan speed possible.

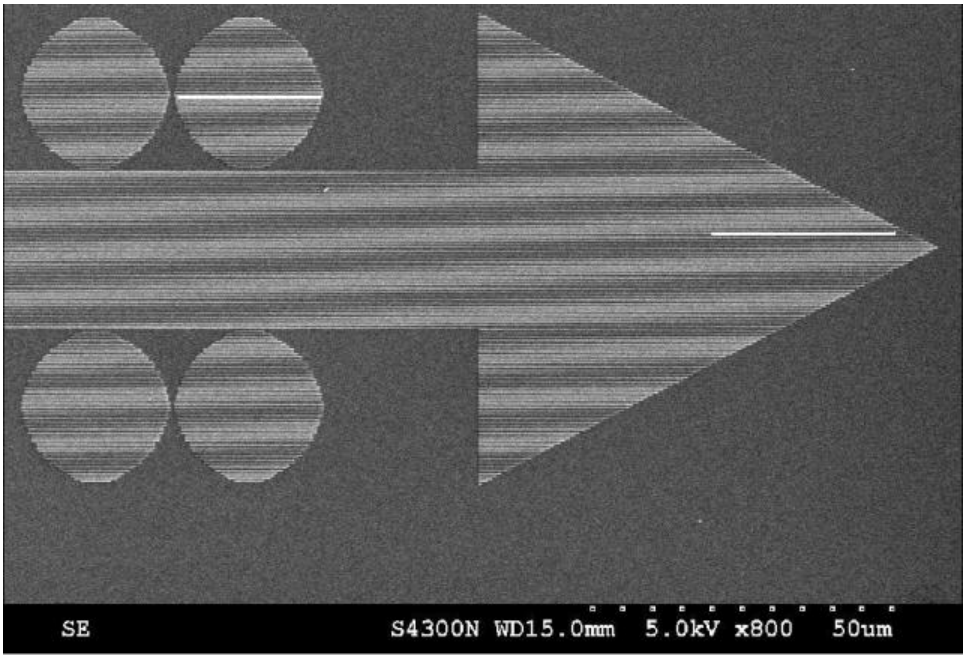

Figure 28: Moiré fringes exhibiting non-linearity in the raster scan at magnification 500x

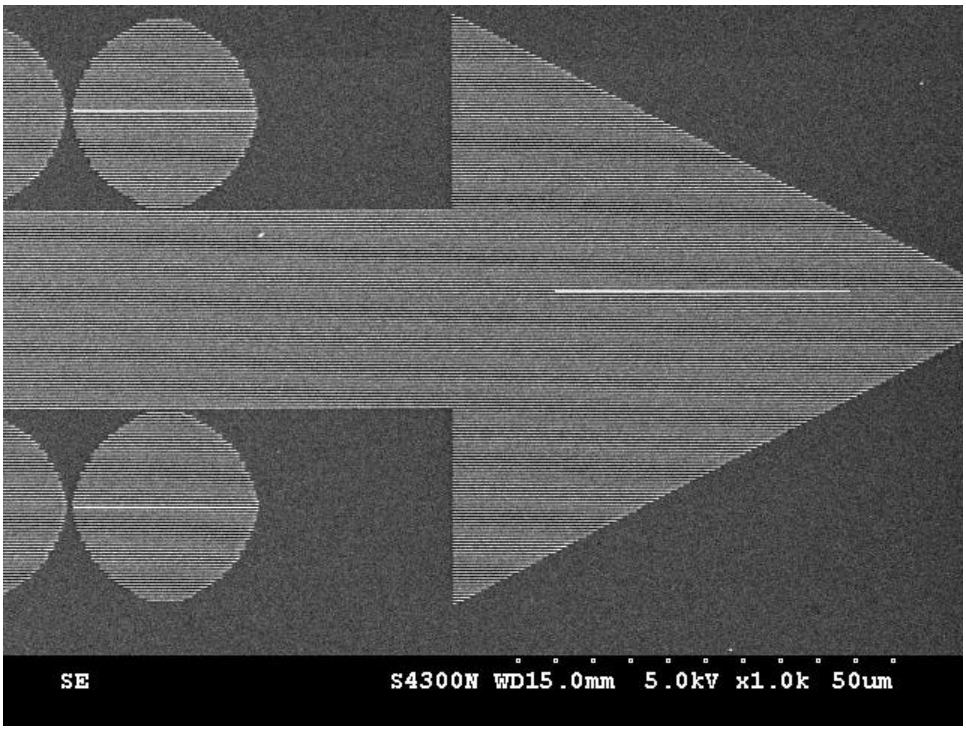

Figure 29: Moiré fringes exhibiting non-linearity in the raster scan at magnification 1.0Kx

It is observed from our experiments that working distance plays a vital role in the non linearity of the raster scan. Increasing working distance leads to decrease in the demagnification. Also the focal length and spot size increases as result of the increasing working distance. Hence image distortion is inevitable at higher working distance. Figure 30 through Figure 32 show examples of distortion observed at different working distances and magnifications. It can be observed from Figure 30 and Figure 31 that at the longest possible working distance can produce a better image (considerably low distortion) than at shorter working distance

Scan non-linearity along either one of the axes can also affect the image to a large extent. The image seen on the display screen need not be the perfect magnified replica of the actual sample structure. The non linearity in any single axis will distort the structure in that particular direction i.e., if seen in x-axis, it would result in stretching the structure (i.e. dynamic changes in the magnification) only along x-direction. Similarly non linearity in y axis would affect the structure only along y direction alone. A circular disk structure viewed at various magnifications is observed to be elliptical in shape. Figure 32 exhibits one of the circular disk patterns captured in the SEM. When measured using Image J software the disks are observed to be elongated along y direction making it look like elliptical, indicating the non-linearity – or possibly an absolute difference in magnification – along y-direction of the raster scan. Therefore raster scan non linearity cannot be ignored, especially while dealing with the measurement using SEM. There are chances to be deceived by the misinterpreted images due to raster scan non linearity.

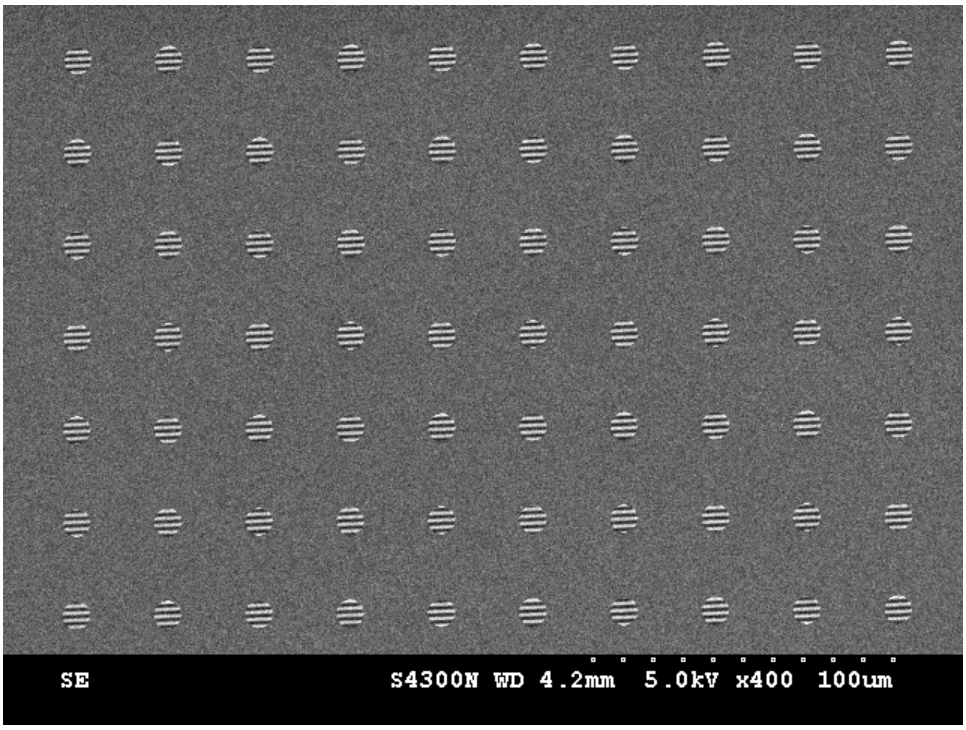

Figure 30: Moiré fringes at the lowest working distance exhibiting maximum non linearity

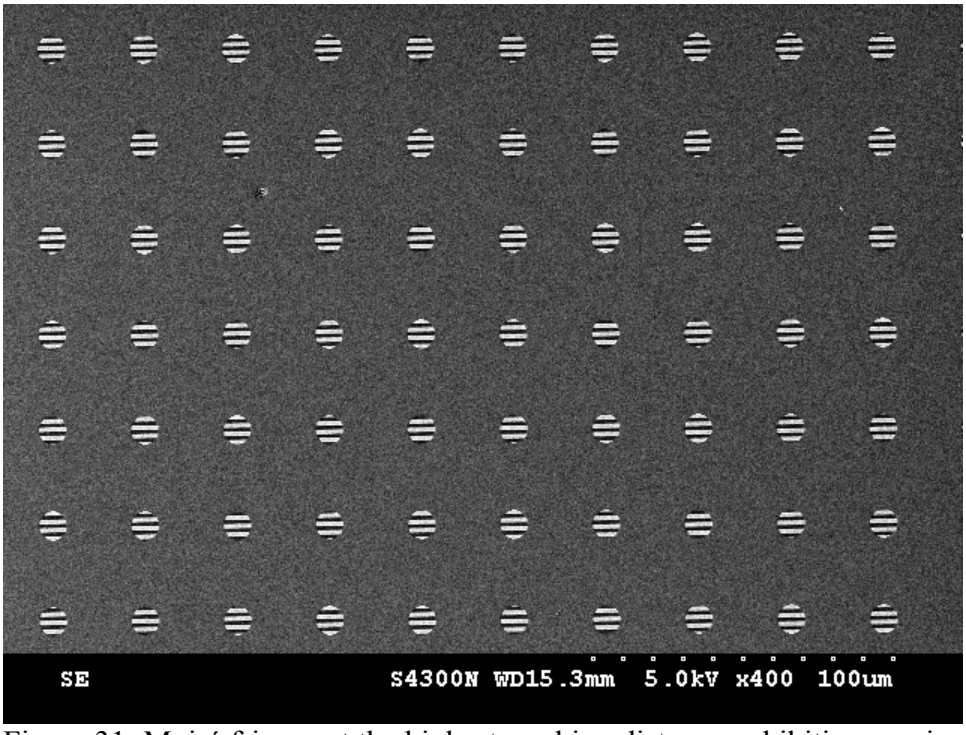

Figure 31: Moiré fringes at the highest working distance exhibiting maximum non-linearity

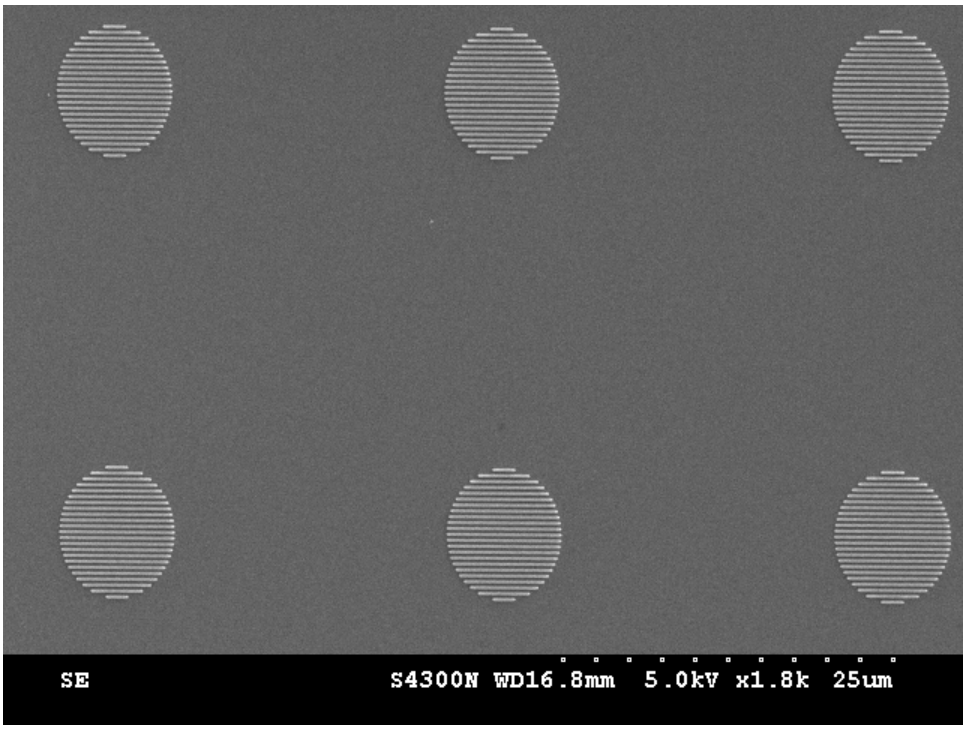

Figure 32: Distortion in the structure of the pattern due to non linearity in the raster scan

4.4 Orthogonality of the raster scan

For the mapped image to be geometrically correct the two axes of the raster scan must be exactly orthogonal. If two axes are not orthogonal, distortion in the images is inevitable. Figure 33 through Figure 35 are used to illustrate the type of distortion that can be expected in case of non-orthogonality of the raster scan. Figure 33(a) and Figure 33(b) illustrates the chess board pattern expected at orthogonal and non-orthogonal raster scan axes respectively. In figure 34, the pattern containing couple of squares (two squares in dark color and two squares in light color) inside a square is examined. The shape that appears in Figure 34 is not a perfect square and to prove this fact, the pattern is overlapped by horizontally flipping the same image, as shown in Figure 35. From Figure 35, it is evident that the axes are not perfectly orthogonal.

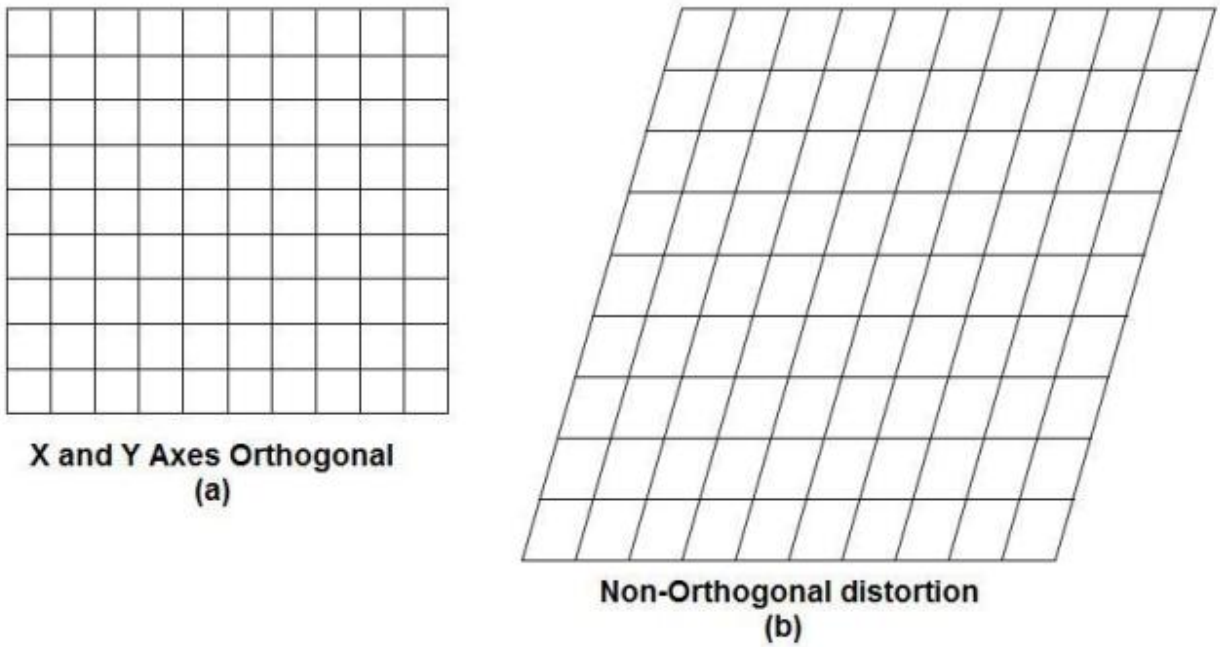

Figure 33: Model of orthogonal non linearity of raster scan

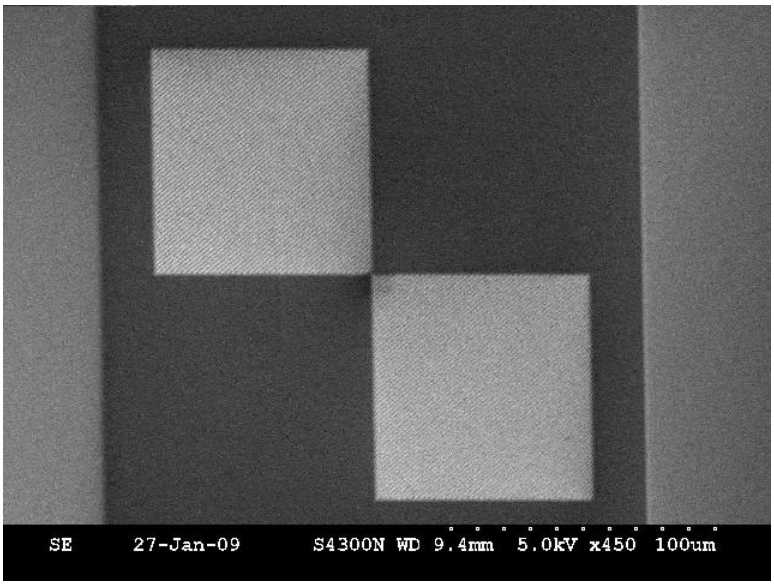

Figure 34: Pattern exhibiting the orthogonal non linearity in the SEM

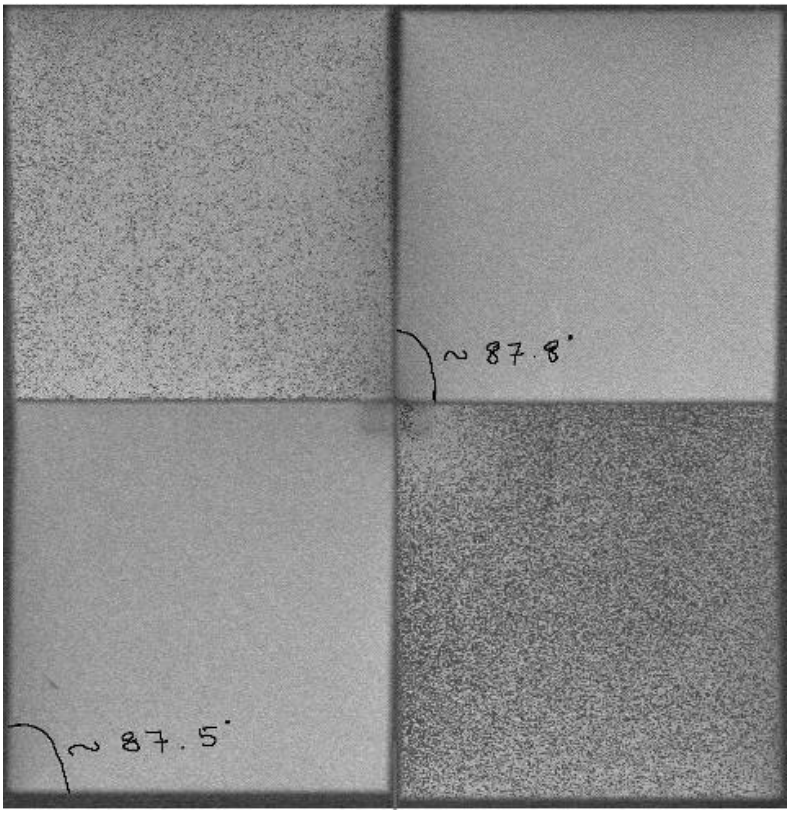

Figure 35: Pattern exhibiting the orthogonal non linearity in the SEM
(Angles measured using Image J are indicated)

4.5 SEM Center offset Calibration

The Center offset (i.e. the beam position in the absence of X and Y scan deflections) of the SEM is important, since the image shift with the changing magnification can cause huge errors in the measurement of the patterns. Usually the center shift is not expected in a perfectly calibrated SEM. Once the specimen is focused at lower magnification, the increase in magnification should not allow any deflection in the beam as the excitation of the objective lens remains unchanged. To investigate the possibility of center shift in the SEM, a special pattern fabricated (by MetroBoost) for center shift calibration was observed while increasing the magnification in steps of 10Kx from 10Kx to 100Kx. Figures 36 through Figure 39 are images at magnifications 90Kx and 100Kx have exhibited shift in the center with increase in magnification. Figure 39 is obtained by overlapping the transparent image of pattern at 90Kx over the same image captured at 100kx. The center shift in pattern in Figure 39 is clearly noticeable. When measured the shift in the center of the images by using image J software, it is observed that the pattern has shifted by 126nm in 'X' direction. In regular practice, the pattern structure which is uniform through out the sample needs a careful observation to avoid errors in measurement. As a center shift cannot be easily identified by the tool or by the software, detection and calibration of this effect is very important.

4.6 Charging and Contamination affects

High scan speeds can provide one of stabilizing charging but adversely affects the signal to noise (S/N) ratios. It can be seen in Figure 36 through Figure 39 that large systematic errors in feature size measurements are associated with this method. Figure 35 is captured at high scan speed (noticeable S/N ratio) and in Figure 37 at slow scan speed (noticeable charging affect).

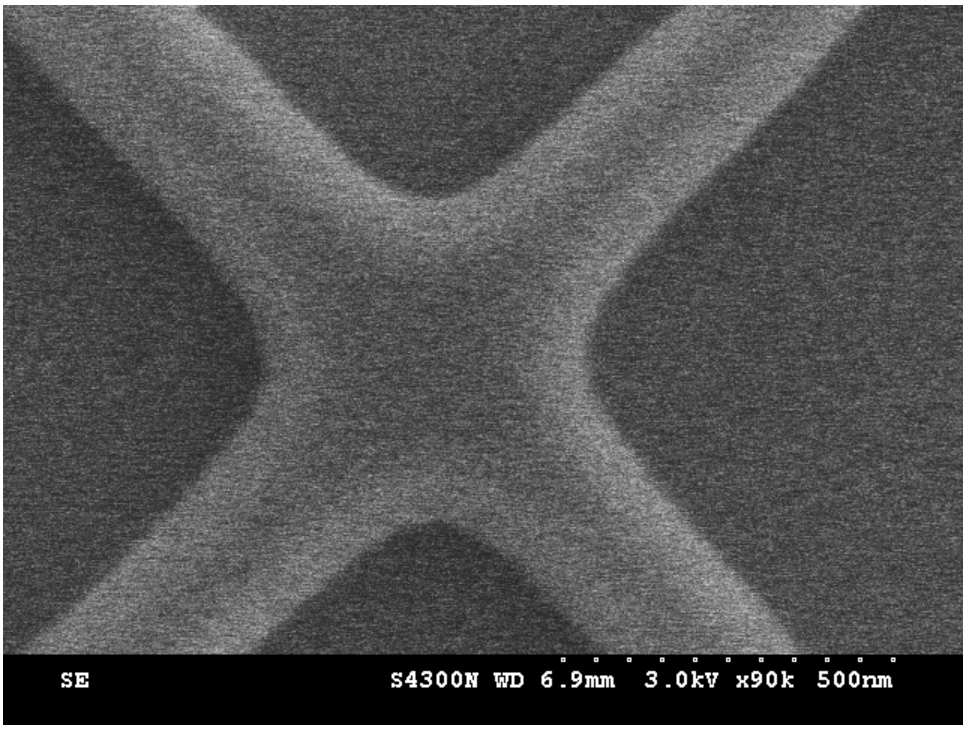

Figure 36: Center shift determination at magnification 90Kx (high scan speed)

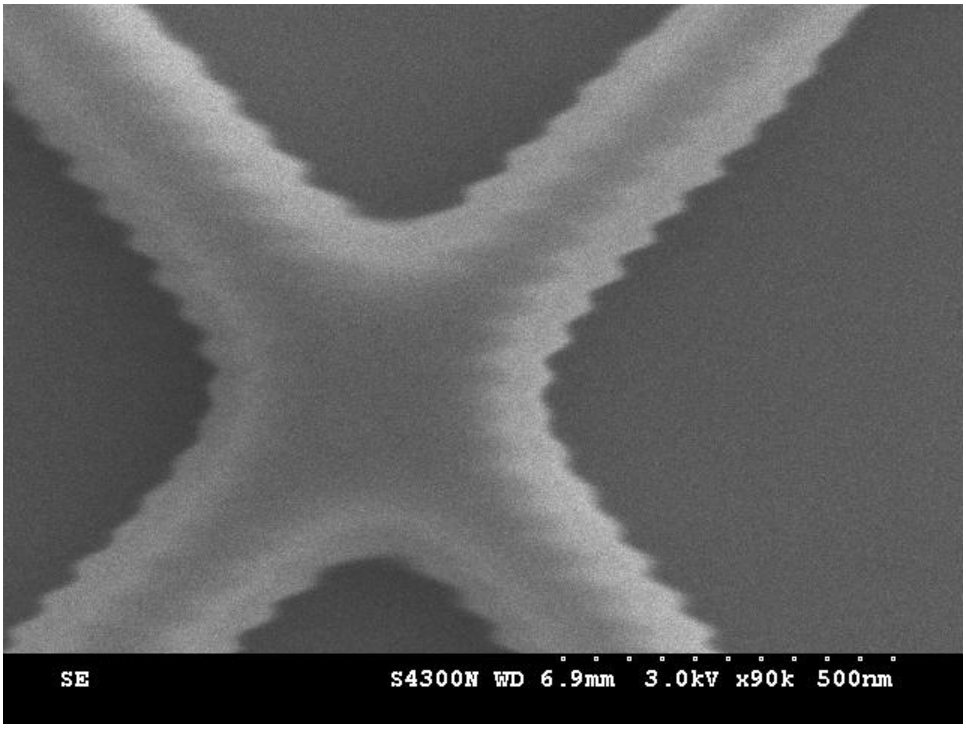

Figure 37: Center shift determination at magnification 90Kx (slow scan speed)

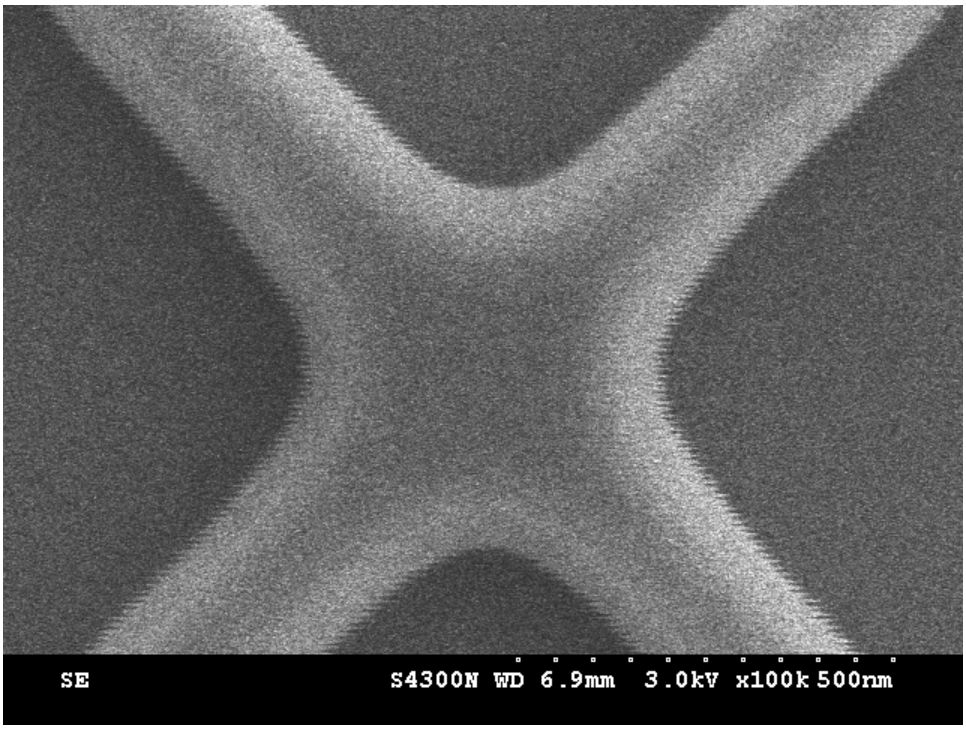

Figure 38: Center shift determination at magnification 100Kx

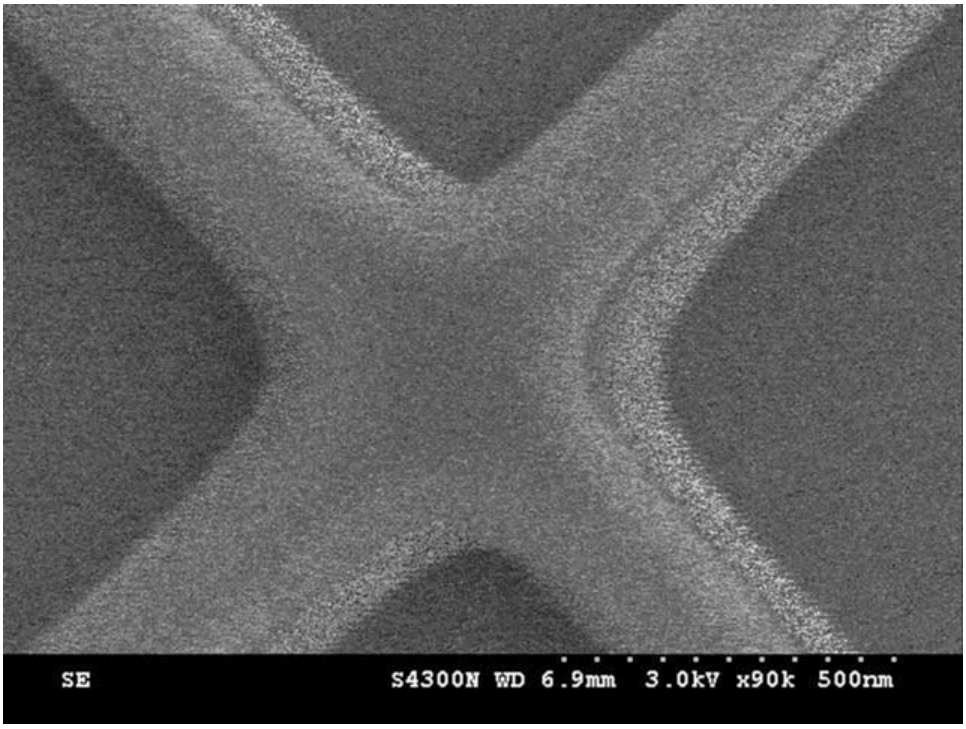

Figure 39: Image formed by overlapping the two center images

The sample with line grating pattern contaminated with dust particle is utilized to study the affect of charging on the pattern by moiré fringe technique. Distortion and irregularity in the moiré fringe periodicity is recorded due to contamination and charging of the sample. Figure 39 through Figure 41 shows effect of charging on the sample. The damage caused on specimen surface due to contamination and charging affect in Figure 39 through Figure 41 is highlighted with a rectangle box around the affected region. In Figure 39, region in the pattern away from the contamination produced moiré fringes with regular spacing. But the contaminated region and area close to contamination that are exposed to more charging affect generated the moiré fringes with irregular fringe spacing. Similarly Figure 40 and Figure 41 shows the marks that have been left on the particular regions of the sample due to charging affect, when beam is focused more on these respective regions(with in the rectangle box in Figures). Sophisticated cleaning techniques such as plasma cleaning, ultrasound cleaning need to be performed to retrieve the affected surface to its original condition. From these results it is evident that contamination and charging affects distort the shape and size of pattern and do have their influence on the measuring capabilities of the SEM. Also from the results discussed in all the above sections, Moiré fringes are found to be a great technique to identify the mapping errors in SEM.

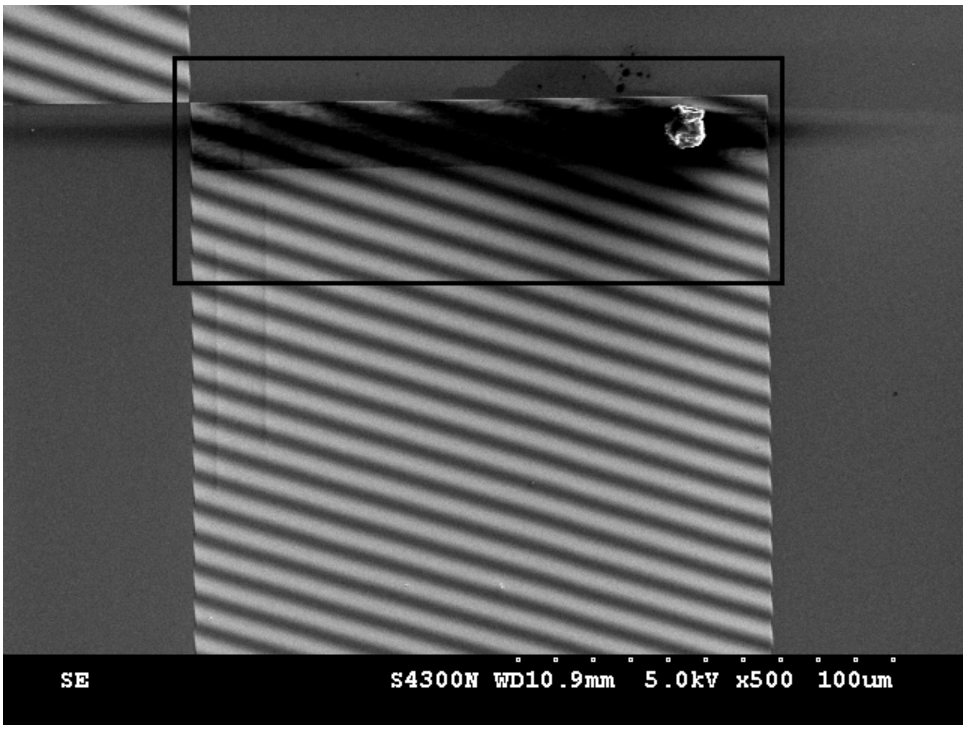

Figure 40: Moiré fringes behavior due to contamination

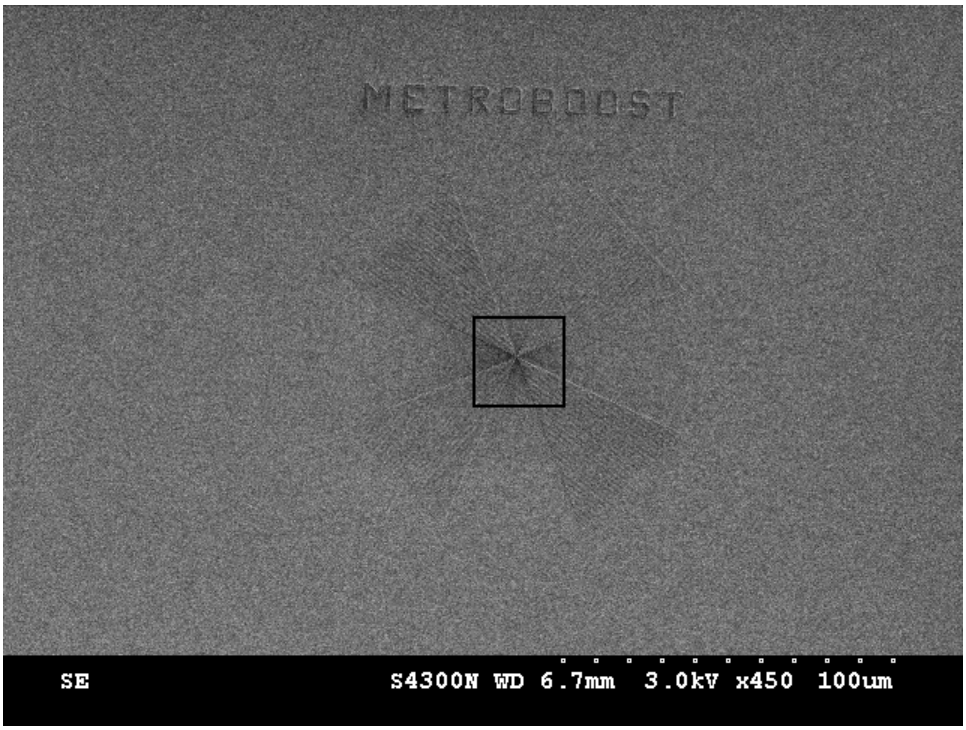

Figure 41: Charging affect seen in the center of the image as a dark patch

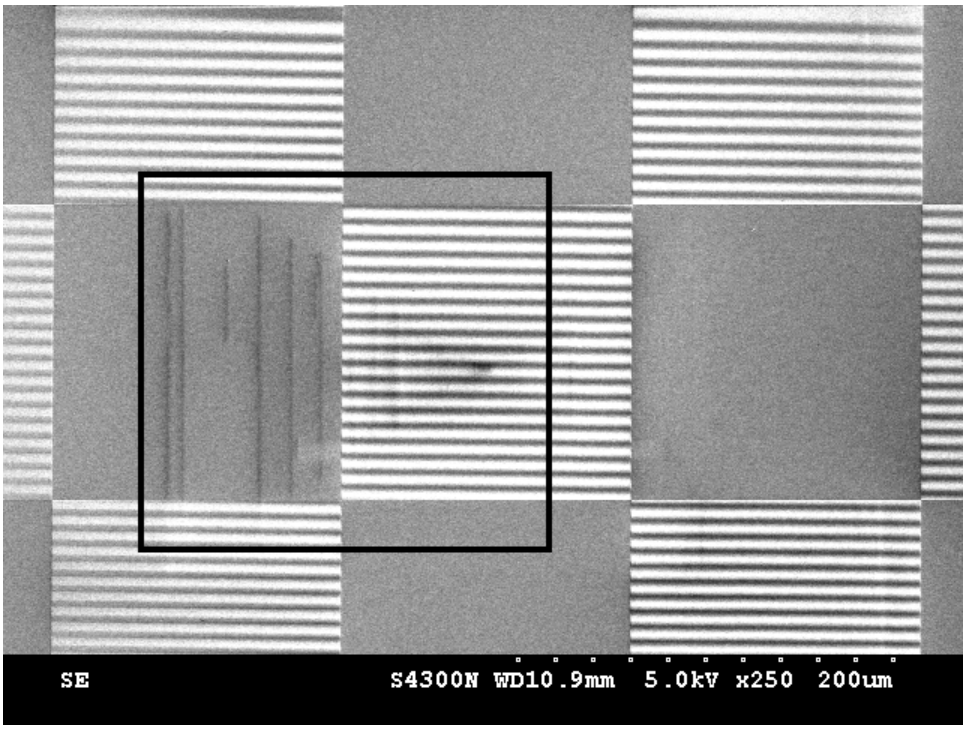

Figure 42: Charging affect shown inside the rectangle.

CHAPTER 5

CONCLUSIONS

Scanning electron microscope is the most widely used tool in many areas of science for measurement purposes, hence the calibration of the SEM is a very important task to be carried out to assure the accuracy of measurement. SEM image based metrology is the most commonly used method for measurement and relies on the assumption that the raster scan mapping is perfect. However, although it is known that there are errors in the SEM raster scan, little efforts have been made to identify the origin, nature, and effect of these errors.

The work presented in this thesis has concentrated on identifying the mapping errors of the raster scan using a novel technique based on the moiré fringes formed by the mismatch between the line grating features in the sample and the raster scan lines. The moiré fringes have also been used to reveal the charging and contamination effects on the pattern shape and size. Evidence of the Non-linearity and non-orthogonality of the raster scan lines have also been obtained and explained by appropriate examples for each case. It can be concluded from these experiments that the moiré fringes can be of great use in understanding the details and problems of quantitative imaging in the SEM.

In addition to identifying the errors in raster scan, behavior of moiré fringes for varying magnification can be used to provide accurate calibration of the imaging field of view (i.e. magnification calibration). The null condition and null magnification formed due to moiré fringes provide a great incentive to fabricate a standard reference artifact for calibration. Since the range of magnification control on the present SEM was limited, null magnification could not be achieved, but nevertheless moiré fringe technique has been utilized to the maximum extent

possible to reveal and quantify the mapping errors that exist. From the results obtained by experiments conducted to identify the non-linearity and non-orthogonality, it can be concluded that the shape, size and orientation of the pattern structure are affected.

In order to reduce the mapping errors likely to be encountered in an SEM, the following suggestions are proposed.

a) To use electrostatic field scanning rather than magnetic scanning detectors: Magnetic scanning suffers from the large back EMF generated at high scan speeds which adversely affects the quality of the raster deflection from the amplifier. Electrostatic scanning generates no back voltage and can therefore stay linear even at the high scan speeds,

b) Scanning the specimen with Piezo or stepper motors, under the control of a laser interferometer, while maintaining the electron beam stationary. This provides ideal linearity and absolute positional accuracy directly traceable to the wavelength of the light used. Drawbacks include cost relative slowness, and complexity.

Tools and techniques such as Atomic force microscope (AFM) and Scanning tunneling microscope (STM) can be considered to be in similar category as SEM, which use similar scanning techniques. The mapping errors identified and solutions proposed in the present work are equally applicable and important for these instruments.

REFERENCES

1. Ausschnitt CP, Lagus ME. IBM Advanced Semiconductor Technology Center, Proc. SPIE Vol3332: p.212 (1998);

2. Michael T.Postek , Robert D.Larrabee , "Submicrometer Linewidth Metrology "

3. Yu Guan and Marco Tortonese, "Metrology Standards for Semiconductor Manufacturing", Solid-State and Integrated Circuits Technology 2004. proceedings 7th international conference,(2004) , Vol – 1, 588-593

4. Metrology , http://en.wikipedia.org/wiki/Metrology

5. Kim Carneiro, Draft report on "The need for metrology in nanotechnology", Danish Institute of Fundamental Metrology, Denmark.

6. Michael Dunlap, J.E.Adakaveg "Introduction to Scanning Electron Microscope", Facility for Advanced Instrumentation, U.C. Davis

7. David C Joy, SEM Lecture notes, University of Tennessee Knoxville.

8. http://www.nationmaster.com/encyclopedia/Metrology

9. Stephen Knight, "Development of Metrology at NIST for Semiconductor Industry", CP638, Characterization and metrology for ULSI technology: 2003 International Conference.

10. David C Joy, "Overview of CD – SEM and beyond" CP638, Characterization and metrology for ULSI technology: 2003 International Conference.

11. Odeb Kafri , Ilana Glatt " The Physics of Moiré Metrology"

12. Alain C Diebold, "Metrology requirements and the limits of the measurement technology for the semiconductor industry", Characterization and metrology for ULSI technology: 2003 International Conference

13. Stephen Knight, Ronald Dixosn, Ronal L.Jones, Eric K.Lin, Ndubuisi G Orji, R.Silver, John S. Villarrubia, Andras E.Valdar, Wen-li Wu "Advanced Metrology needs for nanoelectronics lithography" , S.Knight et al., C.R.Physique 7(2006) 931-941

14. "International Technology roadmap for semiconductors",2007 edition, Metrology

15. Herschel Marchman, "Scanning electron microscope matching and calibration for critical dimensional metrology", Journal of vacuum science and technology B, vol 15(2), (1997).

16. David C Joy, Yeong-Uk Ko, Justin J Hwu, " Metrics of resolution and performance for CD SEMs" , EM Facility, University of Tennessee, Knoxville, TN 37996,Oak Ridge National Laboratory, Oak Ridge, TN 37831

17. Hideaki Abe, Akira Hamaguchi, Yuichiro Yamazaki, "Evaluation of CD SEM Measurement Uncertainty using Secondary Electron Simulation with Charging Effect", Proc. Of SPIE Vol.6518, 65180L,(2007)

18. J.S.Villarrubia, A.E. Vladar, M.T.Postek, "Scanning Electron Microscope dimensional metrology using a model-based library", SURFACE AND INTERFACE ANALYSIS, *surf. Interface Anal.* 2005 ; vol 37: 951-958

19. Olof Bryngdahl, " Moiré : Formation and interpretation", Journal of optical society of America, 1974 ,Vol 64(10), pg no: 1287

20. K. Creath and J.C Wyant " Moiré and Fringe Projection techniques", Optical Shop Testing, Second Edition , 1992,John Wiley & Sons, inc.

21. David T.Read, James W.Dally , " Theory of Electron Beam Moiré" , Journal of research of the national institute of standards and technology , Vol 101,(1),pg 47(1996)

22. David C Joy, Sachin Deo, Brendan J Griffin, "Length calibration standards for nano-manufacturing", Proceeding of SPIE, Vol -6648,664807-1(2007)

23. Fei Su, Jun Wei, Yuchan Liu, " Removal of AFM moiré measurement errors due to non linear scan and creep of probe", Singapore Institute of Manufacturing technology, nanotechnology vol 16(2005) ,pg 1682 -1686

24. Metroboost: Metrocal calibration sample wafer description manual.

25. Joseph I. Goldstein, Dale E. Newbury, Patrick Echlin, David C. Joy, S.D. Romig Jr. and Eric Lifshin. "Scanning electron microscopy and X-ray analysis"

26. http://rsb.nih.gov

VITA

Satyavani Bari was born in city Hyderabad, Andhra Pradesh, India on December 3rd 1982. She did her schooling in Hyderabad. She completed her Bachelors of Engineering in Mechanical Engineering major from Osmania University in June 2004. In January 2005, she started her Master's of Science in Material Science Engineering at University of Tennessee, Knoxville. Under the tutelage of Dr. David C Joy, she has been working in field of nanofabrication, with concentration on nanometrology.